Received: 26 August 2020 | Revised: 16 October 2020 | Accepted: 20 October 2020

DOI: 10.1002/eng2.12327

REVIEW

WILEY

Designing the future atomic electrocatalyst for efficient energy systems

Mingzi Sun | **Tong Wu** | **Bolong Huang**

Department of Applied Biology and Chemical Technology, The Hong Kong Polytechnic University, Hung Hom, Hong Kong SAR, China

Correspondence
Bolong Huang, Department of Applied Biology and Chemical Technology, The Hong Kong Polytechnic University, Hung Hom, Kowloon, Hong Kong SAR, China.
Email: bhuang@polyu.edu.hk

Funding information
National Natural Science Foundation of China, Grant/Award Number: NSFC 21771156; Research Grants Council, University Grants Committee, Grant/Award Number: PolyU 253026/16P

Abstract

Following the fast development of electrocatalysts, atomic catalysts have surely become the most frontier research topic in energy supply systems. In varied electrochemical reactions, they have displayed untapped potential for practical applications due to the exceptional performances in both electroactivity and selectivity, ultra-high metal utilization, and flexible substrates. Besides the conventional experimental synthesis strategies and characterization techniques, advanced theoretical calculations and even machine learning algorithms have been introduced to understand and predict the electrocatalysis performances of novel atomic catalysts, supplying the insightful knowledge for the future rational design and synthesis of the atomic catalyst with the desired properties. Therefore, this review will highlight the recent advance achievements in atomic catalysts regarding the atomic catalyst synthesis and applications, covering the mainstream electrochemical process in energy applications. Meanwhile, we also summarize the application of advanced theoretical explorations as valuable references for future electrocatalyst design. Moreover, we will summarize the existing challenges for the practical applications and the prospects of present atomic catalysts.

KEYWORDS

atomic catalyst, catalyst design, electrocatalysis performance, energy conversion

1 | INTRODUCTION

Single atom catalyst (SAC) is a new frontier in catalysis science. It features the atomically dispersed metal atoms on the solid support surface, anchored by the strong metal-support interaction.[1] The anchored metal atoms do not have bonding interaction with each other, and hence the electronic states are distinct from those metal clusters or particles, where strong metal-metal orbital overlap exists (Figure 1). The conventional heterogeneous catalysts usually contain a mixture of the broad size distribution of metal particles, and only the particles with certain sizes can act as the active species while the remaining ones are inert or even favorable for side-reactions.[3] Moreover, the active sites on the nanoparticles are generally enclosed by the relatively inert surrounding atoms and take up only a small portion of the surface.[4] Therefore, the atom utilization efficiency and selectivity of conventional heterogeneous catalysts are usually poor, leading to unsatisfactory

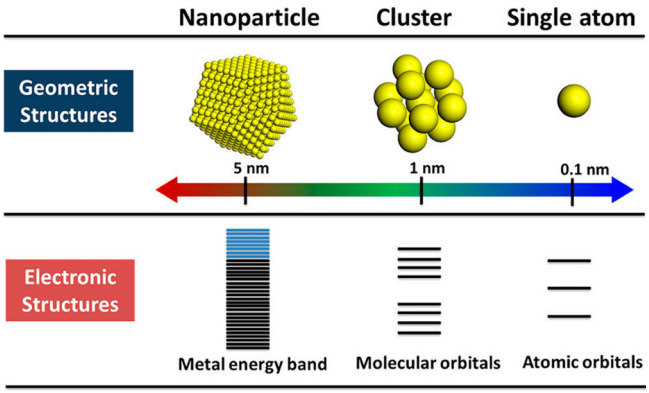

FIGURE 1 Schematic illustration of geometric and electronic structures of nanoparticle, cluster and single atom as the size downscales. *Source:* Reprinted from Reference 2 by permission from the American Chemical Society

mass activity and low Faradaic efficiency (FE). Homogeneous catalysts, on the other hand, have well-defined active sites and tunable coordination environments, and hence they exhibit excellent activity and exclusive selectivity for a specific reaction. However, it suffers from poor stability and troublesome recycling process. Downscaling the particle size is an efficient way to improve the active site utilization rate as the surface-area-to-volume ratio increase and more active sites are exposed on the surface. Nano-engineering downsizes the particles to nanoscale and obtains tremendous properties optimizations through the size-effect. Following this principle, the ultimate downscaling will reach the atomic-scale, which results in the SAC. SACs inherit the merits of both heterogeneous and homogeneous catalysts and are regarded as the bridge connecting the gap between heterogeneous and homogeneous catalysis.[5]

The SAC usually possesses distinct and outstanding performance in many electrochemical reactions, for example, oxygen reduction reaction (ORR),[6-11] oxygen evolution reaction (OER),[12-16] hydrogen evolution reaction (HER),[17-20] nitrogen reduction reaction (NRR),[21-28] and carbon dioxide reduction.[29] The excellent activity of SACs generally stems from the unique single-atom motifs as active sites on the surface. The single atom sites have unique geometry and electronic properties since the metal-metal bonds are absent, and the valence states of the isolated active sites can be tuned by electron-transfer with the anchored support.[17,30] The contribution of SAC to enhance reaction selectivity relies on the unique isolated atom sites on the surface, which show distinct preference to the adsorption configuration of the adsorbates. For instance, the two-electron pathway ORR is more favorable on SACs since the adsorption of O_2 preferably takes the end-on configuration, which favors the formation of OOH* instead of O–O bond cleavage.[31] The strong metal-support interaction not only stabilizes the isolated atoms and prevents the agglomerations, but also substantially modulates the atom electronic state via charge-transfer. This is frequently discussed and demonstrated via characterization techniques and density funcitonal theory (DFT) calculations. A representative example is the Mo^0/GDY SAC, in which the Mo atoms are anchored on the graphdiyne support in zero-valence state.[30] The strong electron-rich environment of GDY preserves the zero-valence state of Mo through a strong p-d coupling. Reversible Mo-C charge transfer not only suppresses the HER process but also activates the hydrogenation of adsorbed N_2, endowing the highly active and selective electrochemical NRR catalysis performance of the Mo^0/GDY. Interestingly, the Mo^0/GDY also facilitates HER if the N_2 is absent from the solution. The HER takes place in the C sites adjacent to the Mo atoms, and the activity also stems from the reversible electron transfer through the p-d coupling between Mo d-orbitals and C p-orbitals. Therefore, the mono-dispersed atom sites of SACs not only achieve the utmost utilization of active sites but also provides innovative pathways to modulate the electroactivity for outstanding electrocatalytic performance.

The minimization of particle sizes to the atomic level inevitably elevates the surface energy to a very high level, where the tendency of atom aggregation and agglomeration into clusters or even large particles is remarkably strong. This is an essential challenge for the synthesis of stable SACs. The rapid developments of synthesis techniques and powerful theoretical modeling have resulted in a variety of systematic approaches to stabilize the single atom sites on the surface via the strong metal-support interaction.[32] Multiple synthesis approaches of SACs have been developed, such as the wet-chemistry approach,[33-35] metal–organic frameworks (MOF)-derived methods,[36-39] pyrolysis,[40] atom trapping,[41-43] electrodeposition,[44] impregnation,[45,46] and so on.

In this minireview, the recent advanced synthesis techniques and strategies for SACs will be first introduced. The characterization techniques of SACs will be briefly discussed subsequently. The electrochemical applications of SACs in HER, OER, ORR, NRR, and CO_2RR are then introduced and discussed. The interpretation of the enhanced and outstanding electrocatalytic activity of SACs and the rational design principles of SACs for each reaction will be the main focus of discussion. Finally, we will present a discussion and outlook for the SAC-related important concepts and future development of SACs. The concept map is given to visualize the topics in the article (Figure 2).

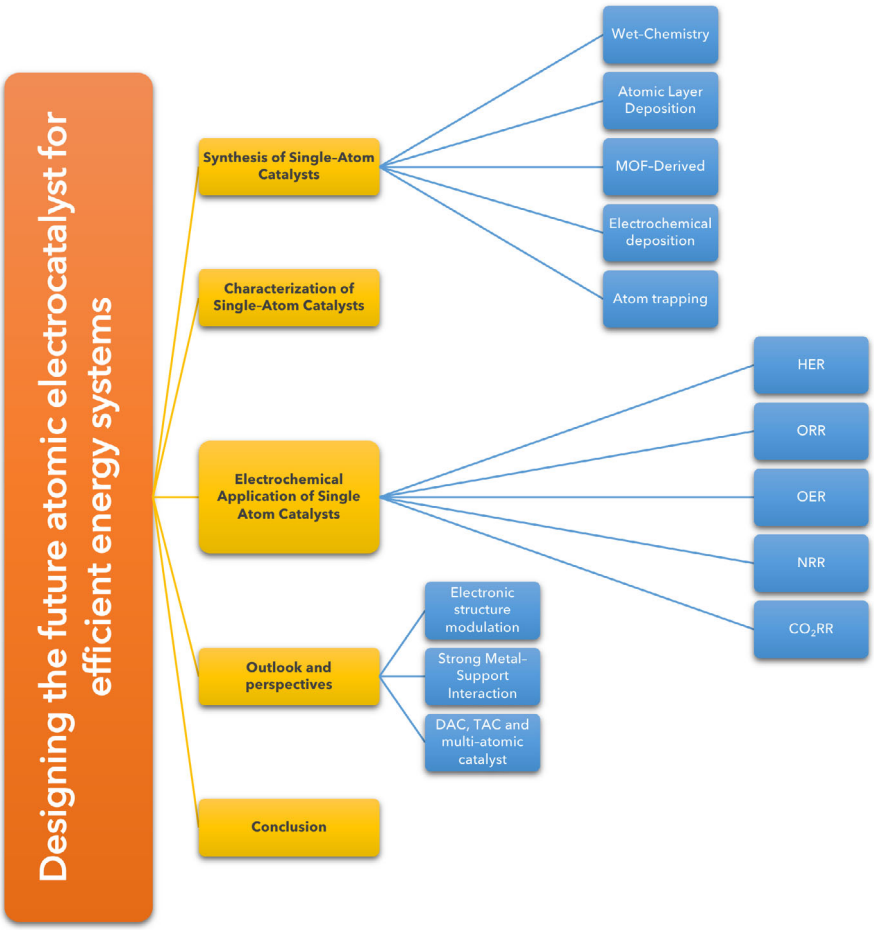

FIGURE 2 The concept map of this review article

2 | SYNTHESIS OF SINGLE-ATOM CATALYSTS

Due to the unique surface structure, preventing the aggregation of metal atoms is the key challenge to synthesize robust and high-performance SAC. Numerous methods have been applied to construct SAC, including the wet-chemistry method,[33-35,47] atomic layer deposition (ALD),[48] MOF-derived method,[49] electro-deposition method,[44] atom trapping,[41-43] and so on. The representative methods will be briefly introduced in the following sections.

2.1 | Wet-chemistry synthetic methods

The wet-chemistry method generally involves three steps to produce SACs. First, the metal species are introduced on various supports via impregnation and coprecipitation. Then, drying and annealing of the materials are done, and finally the reduction or activation of metal species. Theoretically, SACs are achieved by reducing the metal species content to a fairly low level. The smaller particle size will lead to larger surface energy and stronger aggregation tendency. Hence, an effective embedding of metal atoms in support is required for the wet-chemistry method to produce SACs.[50] However, the advantages and disadvantages of the wet-chemistry method are both obvious. On the one hand, it is effective for the synthesis of SAC on oxide substrates, and suitable for potential large-scale production of supported metal catalysts since it does not require specialized equipment. On the other hand, the wet-chemistry method has difficulties in preparing high metal loading materials. Li et al synthesized a Pt SAC anchored on g-C_3N_4 (Pt-CN) catalyst for HER via the wet-chemistry method, in which the Pt loading is only 0.16 wt%.[51] Yang et al reported the synthesis of Pt_1/TiC and Pt_1/TiN SACs by the incipient wetness impregnation method, with the loading of 0.45 wt% and 0.35 wt% respectively.[52]

The SAC synthesis via the wet-chemistry method has developed a number of systematic strategies to achieve atomically dispersion and prevent the as-formed single atoms from migration and agglomeration. The strategies mainly include defect engineering, spatial confinement, and coordination design strategy.[32] The defect engineering strategy exploits

controlled construction of defects on support to trap the metal precursors and anchor metal atoms during post-treatment. The defect engineering enables metal loading control with the concentration of defects and endows the SAC with more property modulations brought by the formation of defects. The typical cation vacancy defect has been used for synthesizing SAC. For instance, by employing defect-rich $Ni(OH)_x$ nanoboards with abundant Ni^{2+} as a support, a high Pt loading (up to 2.3 wt%) SAC was successfully synthesized.[53] In comparison, when the perfect $Ni(OH)_2$ was used, only Pt nanoparticles with a much lower loading of 0.9 wt% were formed. X-ray absorption spectrometry (XPS) and DFT calculations unveiled that the stabilization effect of Ni vacancies contributed to the high metal loading and stability of Pt SACs via an enhanced charge-transfer. The spatial confinement strategy utilizes molecular-scale cages to prevent atom migration. It first encapsulates the mononuclear metal precursors with porous materials such as zeolites, MOFs, and covalent organic frameworks (COFs), and then remove the ligands of precursors by post-treatment to form single metal atoms stabilized by the skeletons of supports.[32] For the coordination design strategy, the coordination sites are rationally designed to capture the metal precursors or atoms to inhibit the migration and agglomeration of metals. The strong interaction between metal species and lone-pair electrons on coordinating atoms such as N, O, and S anchors the single atoms and enables the synthesis of SACs.[2,54,55] For instance, the N sites of tetra(4-(imidazole-1-yl)phenyl)porphyrindine (TIPP) ligands were designed to catch and separate Co^{2+} ions. Followed by pyrolysis, single Co atoms were anchored by surrounding N atoms (Figure 3A).[56] Similar to the defect engineering strategy, the precise control of uniform coordination sites on supports is the prerequisite of the coordination design strategy, which demands fine control of the synthesis conditions.

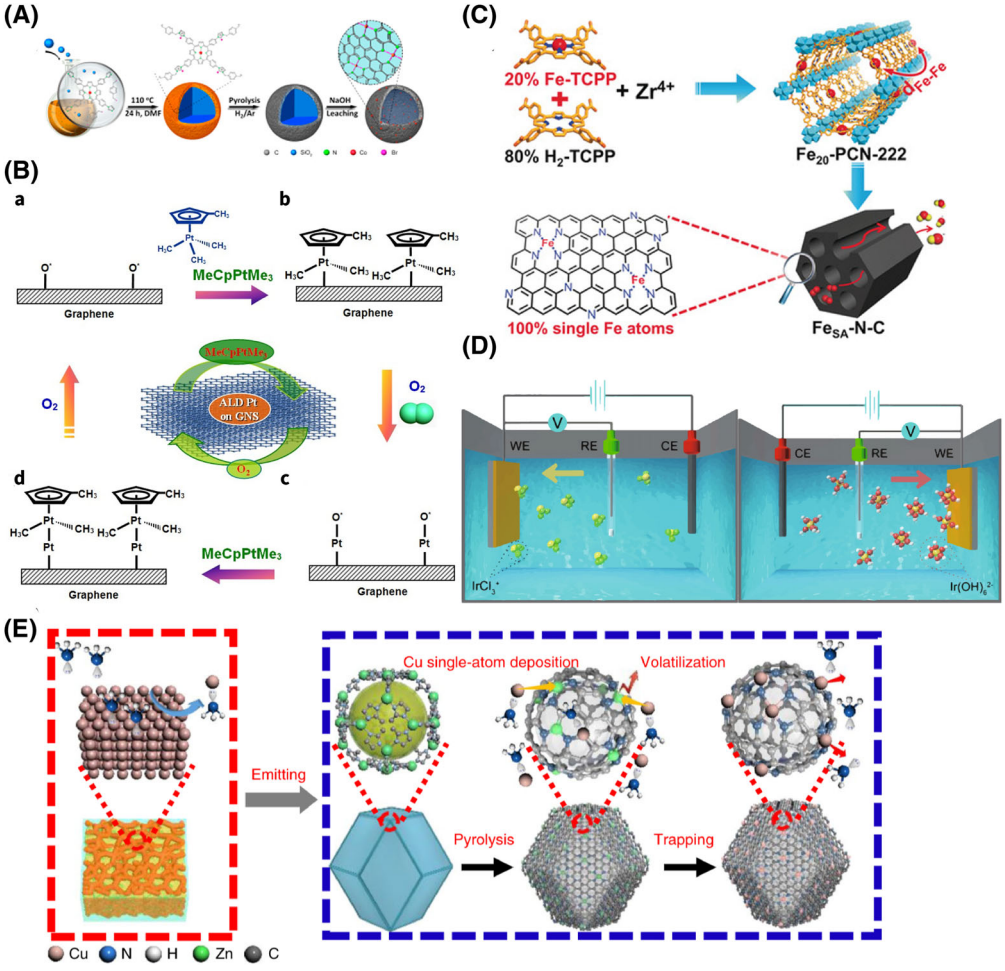

FIGURE 3 The representative synthesis methods for SACs. (A) Schematic illustration of the synthesis of ISAS-CO/HNCS. *Source:* Reprinted from Han et al[56] by permission from the American Chemical Society. (B) Schematic illustrations of Pt ALD mechanism on graphene nanosheets. *Source:* Reprinted from Sun et al[57] licensed under CC-BY. (C) Illustration of the rational fabrication of single Fe atoms-involved Fe_{SA}-N-C catalyst via a mixed-ligand strategy. *Source:* Reprinted from Jiao et al[9] by permission from Wiley-VCH Verlag GmbH & Co. KGaA, Weinheim. (D) Schematic illustrations of cathodic (left) and anodic (right) deposition of Ir species. The yellow, green, red, and white spheres represent Ir, Cl, O, and H atoms respectively. *Source:* Reprinted from Zhang et al[44] licensed under CC-BY. (E) Proposed atom trapping reaction mechanism for the synthesis of Cu-SAs/N-C. *Source:* Reprinted from Qu et al[42] licensed under CC-BY

2.2 | ALD method

ALD is defined as synthesis using alternating and saturating gas-solid reactions, coinvented by two groups working independently.[58] The ALD has been recognized as an effective method at controlling metal and metal oxide sites and improving catalytic activity, selectivity, and durability. It provides a controlled method for atomically precise growth, which is suitable for the synthesis of SACs with metal oxide thin films as support. Sun et al synthesized a Pt SAC anchored on graphene nanosheet using the ALD technique for the first time (Figure 2B).[57] The synthesis procedure starts with oxygen atoms implanted in graphene nanosheets, which can react with (methylcyclopentadienyl)trimethylplatinum ($MeCpPtMe_3$). The organic ligands of $MeCpPtMe_3$ are converted into H_2O, CO_2, and hydrocarbon fragments under exposure to O_2, leading to the formation of Pt-containing monolayers. The remaining O_2 oxidized the Pt-containing monolayers to form a new absorbed oxygen layer on the Pt surface, which will subsequently react with the new MeCpPtMe to initiate the next cycle. This is the whole ALD cycle in preparation for the Pt SACs on graphene nanosheets. Controlling the number of ALD cycles will adjust the morphology, size, and loading weight of Pt SACs. The ALD method provides a powerful method for the synthesis of noble metal SACs on several types of supports, such as SiO_2, Al_2O_3, and TiO_2.[48,57,59-61] However, the low yields, the high expense of equipment, and precursors of ALD limit its widespread production.[62,63]

2.3 | Metal-organic frameworks (MOF) method

MOFs have received much attention in recent years due to their high specific surface area, tunable porosity, and unique structures. These intrinsic properties would perfectly meet the substrate requirements for stabilizing SACs.[64] The MOFs outperform other conventional porous SAC supporting materials such as zeolites, carbon nanotubes (CNTs), and graphene with its easy and precise control of nanoarchitectures. The desired sizes, porosities, and functional groups of MOFs can be simply controlled by the constituent geometry through synthetic designs. Thus, MOFs are expected to be one of the most promising and versatile platforms for fabricating SACs with high metal loadings and stability.[64] Additionally, MOF-derived materials obtained by pyrolysis partially inherit the structural properties of the original MOF, and hence could also serve as a good alternative support material for SACs.

The MOF-based SACs can be classified into MOF-stabilized SACs and MOF-derived SACs. MOF-stabilized SACs are prepared by direct immobilization of single metal atoms on the MOFs. The tunable pore size and shape of MOFs allow the selective accessibility of reactions substrates or products, endowing MOFs with catalytic selectivity. However, the instability under harsh conditions, for example, electrocatalysis, and its weak conductivity of MOF substrates hinders the applications of MOF-stabilized SACs in electrochemical reactions. For the MOF-derived SACs, the MOFs or MOF-based composites act as the precursors for the synthesis. The metal ions are atomically dispersed in the structure of MOFs by the coordination of organic ligands. For instance, the N-rich ligands in MOFs are utilized as nitrogen and carbon sources to prepare N-doped carbon materials after the pyrolysis. Therefore, the MOF-derived SACs typically endure harsh conditions better than the MOF-stabilized SACs. Moreover, MOF-derived SACs feature excellent conductivity, high specific surface areas, desired hierarchical structure, and maximized atom utilization efficiency, showing the enormous potential in electrocatalysis.[64] Synthetic strategies for MOF-derived SACs mainly include a mixed-metal strategy, a mixed-ligand strategy, and a spatial confinement strategy.

The key to the mixed-metal strategy for SAC preparation is to realize the homogeneous dispersions of two types of metal nodes in one MOF structure, whereas most MOFs have only one kind of metal node or cluster. The mixed-metal MOFs have two types of metal sites. The targeted metal sites are separated by both N-rich linkers and the second metal sites with low boiling points (eg, Zn).[64] The pyrolysis process or annealing will evaporate the second metal sites, leaving the targeted metal species anchored on the derived N-doped porous carbon matrices. The strong N-metal interactions will substantially stabilize the atomically dispersed metal atoms and prevent the aggregations. The zeolitic imidazolate framework (ZIF) is the frequent choice as a precursor for the mixed-metal strategy because the targeted metal besides zinc can be easily introduced into the ZIF. Li et al reported the synthesis of Co/NC SACs with the loading of Co over 4 wt% by pyrolysis of Zn/Co-ZIFs.[65] The limit of mixed-metal strategy is that if the targeted metal atoms cannot assemble the isostructural MOFs precursor, especially for some noble metals that are rarely used as the metal nodes of MOFs.[64]

The mixed-ligand strategy is similar to the mixed-metal strategy. The targeted single metal sites are separated by the different types of ligands, and the coordination environment of the targeted metal sites can be adjusted via the selection of ligands. The distance between the metallated ligands is simply controlled by adjusting the ratio of the mixed ligands. When the distance is appropriate, the immigration of metal atoms is sufficiently inhibited and SACs will form after the

pyrolysis. A successful example of a mixed-ligand strategy is the Fe/NC SACs prepared by direct pyrolysis of a mixed-ligand porphyrinic MOF (Fe_{20}-PCN-222) and a subsequent ZrO_2 removal step (Figure 3C).[9] Notably, the MOF-derived Fe/NC SACs inherits the rod shape and highly oriented mesopores of the precursor Fe_{20}-PCN-222, which contributes to the excellent ORR activity.

Spatial confinement strategy utilizes the pores/cages of MOFs to encapsulate the isolated mononuclear metal precursors, which efficiently suppress the aggregation of nearby metal atoms during the pyrolysis process. The prerequisite is that the molecular sizes of metal precursors must be larger than half of the pore/cage sizes of MOFs to ensure the entire occupation of each cage/pore by only one metal precursor. This also limits the universality of this method to some extent, because most of the conventional metal salts have too small sizes and hence are excluded. Hence, $M(acac)_x$ and ferrocene (Fc) with large ligands are the proper choices for metal precursors. Li et al synthesized a Fe/NC catalyst by pyrolysis of the Fe/ZIF-8, in which the pores are inserted by $Fe(acac)_3$ one-by-one.[66]

The future development of MOF-derived SACs needs to solve the agglomeration of metal atoms at high metal loadings in order to produce the SACs with a higher density of active sites. It is expected that the combination of theoretical modeling and experiments will promote the guided design and synthesis of high metal loading MOF-derived SACs. Efforts must be made in searching the guiding principles and developing essential techniques to achieve the fine control of desired structural and catalytic properties for large-scale industrial applications.

2.4 | Electrochemical deposition

In a recently published work, Zhang et al proposed an electrochemical deposition approach as a universal route for fabricating SAC (Figure 3D).[44] The prevalent SAC synthesis techniques usually have special requirements for either the anchored metals or the supports. For instance, the pyrolysis method generally yields carbon-based support due to the decomposition of metal-organic components.[64] The wet-chemistry method suffers from the trial-and-error process since there is still no consensus that has been reached on the mechanism.[44,46-67] The atom trapping method requires both the mobile metal species and trapping sites on the supports.[41] In comparison, by adjusting the metal precursors and supports, a series of SACs can be successfully obtained from cathodic or anodic deposition. Surprisingly, even for the same metal, the cathodic deposition products and anodic deposition products exhibit distinct electronic states. Consequently, the cathodic deposition SACs are reported to be promising HER catalysts, while the anodic deposition ones are candidates for OER catalysts.

The mechanistic study revealed that the electrodeposition process resembles the molecular mechanism of nucleation in the solution-phase synthesis, where the support can be regarded as the solvent.[44] The upper limit of mass loading for SACs is determined by the minimum supersaturation on the support. When the mass loading exceeds the minimum supersaturation level, the atomically dispersed metal will start to aggregate into clusters. The generality of the electrodeposition method was tested by 4d and 5d metal precursors, including Ru, Rh, Pd, Ag, Pt, and Au, and all of these metals were successfully deposited atomically on $Co(OH)_2$ nanosheets. The method was further successfully extended to 3d and 4d transition metals on nitrogen-doped carbon (N–C) support. In addition, the Ir single atoms were also deposited on various supports such as $Co(OH)_2$ nanosheets, MnO_2 nanosheets, MoS_2 nanosheets, $Co_{0.8}Fe_{0.2}Se_2$ nanosheets, and N–C from both cathodic and anodic deposition. Therefore, the electrochemical deposition is a universal method that is applicable to a wide range of metals and supports for the fabrication of SACs.[44]

2.5 | Atom trapping

Synthesis of SACs with high metal loadings and stable performance at high temperatures is essential for industrial applications. For heterogeneous catalysts made from precious metal nanoparticles adsorbed on metal oxides, high temperatures will make the metal atoms mobile and aggregate into larger particles, which is known as Ostwald ripening process. The catalysts, therefore, suffer from a loss in surface area and activity. The atom trapping method is a desirable novel approach to resolve this issue.

Jones et al innovatively utilized the mechanism and conditions of Ostwald ripening to create SAC.[41] They showed that the conditions under which nanoparticles emit mobile species are also ideally suited to generating atomically dispersed catalysts if the mobile species can be effectively trapped. At 800°C in oxidizing ambient conditions, Pt is emitted as volatile PtO_2, and can be trapped and dispersed atomically with appropriate supports. Ceria is found to be effective for

inhibiting the sintering of Pt and able to trap the Pt in a single-atom state, confirmed by a variety of characterization techniques, for example, X-ray powder diffraction (XRD), energy-dispersive spectroscopy (EDS), and aberration-corrected scanning transmission electron microscopy (AC-STEM). Surface species such as hydroxyls and carbonates, which could prevent the trapping of mobile species, would have desorbed at high temperatures and provide a clean surface for better stabilization of single atoms. Qu et al reported a facile gas-migration strategy to directly transform bulk materials into single atoms onto the support, which has great potential for large-scale production.[42] First, the ammonia coordinates with the copper atoms to form volatile $Cu(NH_3)_x$ species based on the strong Lewis acid-base interaction. Then, following transportation under an ammonia atmosphere, the $Cu(NH_3)_x$ species are trapped by the defects on the nitrogen-rich carbon support, forming the isolated Cu sites. The synthesized Cu-SAs/N-C catalysts show a superior ORR performance and exceptional electrochemical and thermal stability. Additionally, a series of M-SAs/N-C (M = Co or Ni) could be fabricated using this gas-migration method, demonstrating the generality of this approach. Besides trapping the mobile species in the gas phase and high temperature, atom trapping is also viable in ambient conditions. Qu et al described an ambient synthetic strategy to construct SACs from metal foam (metal = Fe, Co, Ni, and Cu) by the surface dangling bonds of graphene oxide (GO) support.[43] When mixing GO slurry with metal foam and drying in ambient conditions, electron transfers occur from M^0 to the dangling oxygen groups on GO, resulting in $M^{\delta+}$ $(0 < \delta < 3)$ species. Meanwhile, M–O bonds are formed as M^{δ} coordinates with the surface oxygen dangling bonds of GO. Subsequently, the metal atoms are pulled out of the metal foam by the M–O bonds under the assistance of sonication to give M-SAs/GO materials. This synthesis at room temperature from bulk metals provides a versatile platform for facile and low-cost fabrication of SACs.

Atom trapping should be broadly applicable as a method for preparing single-atom catalysts. The approach requires a supply of mobile atoms and support that can bind the mobile species. The conditions that are favorable for Ostwald ripening are ideal because mobile species are generated continually.

3 | CHARACTERIZATION OF SINGLE-ATOM CATALYSTS

It is necessary to examine and confirm the existence of single atomic sites. This requires a high spatial resolution to determine the single atoms with several-angstrom sizes. To date, sophisticated characterization tools used for that purpose include electron microscopy, such as scanning tunneling microscopy (STM) and high-angle annular dark-field imaging scanning tunneling microscopy (HAADF-STEM), as well as spectroscopic techniques including extended X-ray absorption fine structure (EXAFS), X-ray absorption near-edge structure spectroscopies, and infrared (IR) spectroscopy.[68] The in-situ/operando characterization techniques are also important to reveal the reaction process and mechanism on SACs as the model reaction systems.[69] The characterization techniques of SACs will be briefly introduced herein.

3.1 | Electron microscopy approach

The development of electron microscopy has reached sub-angstrom scale, endowing the image quality to directly capture the presence of single metal atoms dispersed on support and determine the location as well as the spatial distribution of single atoms.[70,71] HAADF-STEM takes advantage of the Rutherford scattering of electrons to detect heavy atoms on light elements of supports.[72] It has successfully distinguished the single metal atoms for elements such as Pt, Pd, Au, and Fe.[73-77] The disadvantage of HAADF-STEM is that it cannot distinguish the single metal atoms from the support if their atomic numbers are close.[68] When the support is conductive, STM can provide the atomic and electronic structure information of single metal atoms. Deng et al used low-temperature STM images combined with STM simulation to confirm that a FeN_4 center is embedded in the graphene matrix and the iron center significantly modified the density of states of adjacent atoms.[75]

The in situ observation of the electronic states of single metal atoms in a reaction environment is challenging. The recent development of environmental TEM (ETEM) enables the in situ characterization of structural evolution of SACs under gaseous and operational conditions.[78] The in situ TEM with the atomic resolution was first reported by Gai et al[79] The successful applications include the observation of Pt atoms migration,[80,81] transformation between Pt atoms, clusters, and nanoparticles,[82] the transformation of noble metal nanoparticles to stable single atoms at above 900°C,[83] and also the growth of graphene catalyzed by SACs.[84] These results demonstrate the great power of in situ TEM and STM for characterization and reaction tracking of SACs.

3.2 | Spectroscopic techniques

Spectroscopic techniques for SACs characterization mainly involve EXAFS, Fourier transform (FT) spectrum, and IR spectroscopy. The EXAFS spectra data can offer information about the local coordination number, interatomic distances, structural disorder, and kind of neighboring atoms at a given distance.[85] The characteristic feature of SACs in EXAFS spectra is the absence of metal-metal bonds. Chen et al applied the EXAFS successfully to evaluate the sizes of supported Ag NPs and determine the structures of the anchoring sites of single Ag atoms.[77] Similarly, the metal-metal bond amplitude in the FT spectrum will disappear when the metal atoms are dispersed atomically.[86] IR spectroscopy is also able to distinguish and quantify single metal atoms from metal nanoparticles. Yates et al confirmed the presence of single Rh atomic species in their Rh catalysts via IR spectroscopy.[87] Some recent works also differentiate and quantify the fraction of Rh single atoms and Rh nanoparticles.[88,89]

The in situ Fourier transform infrared (FTIR) is able to provide more decisive evidence to exclude the presence of NPs in SACs, which the TEM method could not achieve. The in situ FTIR is highly sensitive to the vibration mode of the adsorbed CO molecule on the active site, distinguishing the nanoparticle sites and single-atom sites and offer effective tracking of the reaction pathways of CO catalyzed on SACs.[69] Qiao et al demonstrate the presence of only isolated and positively charged single Pt atoms in Pt1/FeOx SAC via the characteristic CO adsorption peak at 2080 cm^{-1}.[47] Similarly, the existence of atomically dispersed metal atoms in single-atom alloy (SAA) catalysts. Pei et al distinguished the atomically dispersed Pd sites in the $AgPd_{0.025}/SiO_2$ catalyst reduced at different temperatures by comparing the relative intensity of the CO adsorption bands.[90] Tracking the change of vibrational peaks in situ FTIR, the reaction pathways are detected experimentally. Shan et al observed the development of the C=O stretching peak of acetaldehyde at 1723 cm^{-1} in the nonoxidative ethanol dehydrogenation reaction catalyzed by $Ni_{0.01}Cu$ SAA. The results supported the evidence of the participation of Ni atoms in the cleavage of the C–H bond of ethoxy species at lower temperatures compared to Cu NPs.[91]

4 | ELECTROCHEMICAL APPLICATION OF SINGLE ATOM CATALYSTS

4.1 | Hydrogen evolution reaction (HER)

HER is the fundamental reaction of electrochemical water-splitting and has been widely considered as a sustainable alternative to traditional fossil fuels.[92] HER is a two-electron transfer reaction, and its mechanism and elemental steps are depicted in the following equations:

Volmer step:

$$H_3O^+ + e^- \rightarrow H^+ + H_2O \text{ (acidic solution)} \quad (1)$$

$$H_2O + e^- \rightarrow H^+ + OH^- \text{ (alkaline solution)} \quad (2)$$

Heyrovsky step:

$$H^+ + H^+ + e^- \rightarrow H_2 \text{ (acidic solution)} \quad (3)$$

$$H^+ + H_2O + e^- \rightarrow H_2 + OH^- \text{ (alkaline solution)} \quad (4)$$

Tafel step:

$$2H^* \rightarrow H_2 \text{ (acidic/alkaline solution)} \quad (5)$$

Equations (1) to (5) show that the chemisorption of H* is the key intermediate of the HER, which limits the reaction rate. According to the Sabatier principle,[93] the optimum catalyst should have the Gibbs free energy of H* (ΔG_H) close to zero. Therefore, the development of HER electrocatalysts focuses on the optimization of ΔG_H.

TABLE 1 Summary of HER single atom catalysts

Catalyst	Synthesis	Application	Overpotential (η)	Activity
Ni(0)/Fe(0)/GD[17]	Electrochemical deposition	Acidic HER	66 mV at 10 mA cm^{-2} (Fe/GD)	80.0 A mg_{metal}^{-1} at $\eta = 0.2$ V
Pd^0/GDY[94]	Electrochemical deposition	Acidic HER	55 mV at 10 mA cm^{-2}	61.5 A mg_{metal}^{-1}
Ru/GDY[15]	Electroreduction	Acidic HER	44 mV at 10 mA cm^{-2}	15.88 A mg_{metal}^{-1}
Cu@GD NA/CF[95]	Self-catalyzed growth	Acidic HER	79 mV at 10 mA cm^{-2}	Tafel slope = 69 mV dec^{-1}
Ru/Pt/Pd@Co-SAs/N-C[96]	MOF-derived	HER (all pH)	7 mV at 10 mA cm^{-2} in 1 M KOH (Ru@Co-SAs/N-C)	500 A g_{Ru}^{-1}

In recent years, the emerging SACs have demonstrated their superior HER activity compared to their traditional nano-counterparts, especially in neutral and alkaline conditions (Table 1). More importantly, the choice of metal is no longer limited to limited noble metals. Various earth-abundant transition metals such as Fe, Co, Ni, Mo, and W have been developed as promising alternative materials to Pt for HER.[97] The carbon-based materials and metal compounds are the major choices as the support of the SACs.[97-101] The strong coupling interaction between the support and metal atoms not only prevents the agglomeration of the atoms but also endows unique electronic structure properties to the atom site, contributing to the enhanced activity of HER. Xue et al reported that the zero-valence Ni and Fe anchored on graphdiyne (GDY) SACs were designed and successfully synthesized, exhibiting unique electronic structure properties and superior HER activity.[17] The Fe/GDY exhibits the best HER activity with only 9 mV onset overpotential, and an overpotential of 66 mV at 10 mA cm^{-2}, which is better than the other earth-abundant metal HER catalysts and comparable to the noble-metal-based catalysts (Figure 4A). It even surpasses the commercial Pt/C in terms of mass activity. This superior HER activity is ascribed to the abnormally strong (sp)-d orbital overlapping between the Ni/Fe atoms with the surrounding carbon atoms. With the innovative ab initio method proposed by the co-author Huang,[103-106] the neutral state of the metal atoms is revealed as the result of the compensation of electrons from the sp-orbitals of C, forming the $3d^{8+\delta}$ ($\delta \sim 2$) electron configuration and activating the neighboring carbon atom sites. The electronically active C sites in Ni/Fe anchored GDY system demonstrate moderate ΔG_H around 0 eV, promoting both the adsorption and desorption of H* (Figure 4A). The excellent properties of graphdiyne have led to a number of high performance HER SACs.[15,94,95]

The HER SACs have developed into more complex designs. For instance, metal clusters are imported to the SACs without changing the original isolated dispersion of metal atoms. The imported metal clusters interact with the single atom site, generating a synergistic effect, which enhances the reactivity. Yuan et al innovatively designed and synthesized metal clusters (Ru, Pt, Pd, and so on) combined with single cobalt atoms anchored on nitrogen-doped carbon (Ru/Pt/Pd@Co-SAs/N-C) (Figure 4B).[96] The catalyst demonstrates a superior HER catalytic activity and stability in basic media compared with the commercial Pt/C, and additionally offers an excellent pH-universal HER activity covering acidic, neutral, and basic conditions. Notably, proven by multiple characterization techniques, the uniform monodispersed Co atoms on the surface are not disturbed by the formation of metal clusters. The superior pH-universal HER activity is ascribed to a synergistic effect between the clusters and Co single atom sites, revealed by the DFT calculations. The MOF derived SACs have also attracted great attention in electrochemical catalysis applications, including HER.[18-20]

Besides the experiment efforts, theoretical studies have also been extensively conducted to investigate the rational design principle of SACs for HER. Hossain et al studied a series of transition metals supported on nitrogen-doped graphene as SACs for HER by a combination of DFT calculations and electrochemical measurements.[107] The theoretical screening of ΔG_H shows that only a few of the transition metals (eg, Co, Cr, Fe, Rh, and V) are suitable for HER, in which Co-SAC has the most optimal ΔG_H. They further analyzed the electronic structures and found that only the valence d_{z2} orbital actively participates in the reaction with hydrogen. The superior HER electrochemical activity of Co-SAC was mainly originated from the location of $3d_{z2}$ valence orbital near to the Fermi level and its partially empty antibonding state. Moreover, a linear correlation for the catalytic activity (ΔG_H) with the electronic structure of SACs and charge transfer along SACs was found. They confirmed their theoretical results by synthesizing three SACs (Co, Ni, W) and the experiment results were aligned with the prediction that Co-SAC would be the best HER catalysts while both of them exhibited superior HER activity. Huang et al conducted a theoretical study of TM SACs based on AX (A = Al, Ga, In, and Tl; X = S and Se), BX_2 (B = Mo and W) and ZrS_2 monolayer substrates for HER in order to find out the efficient HER activity descriptor

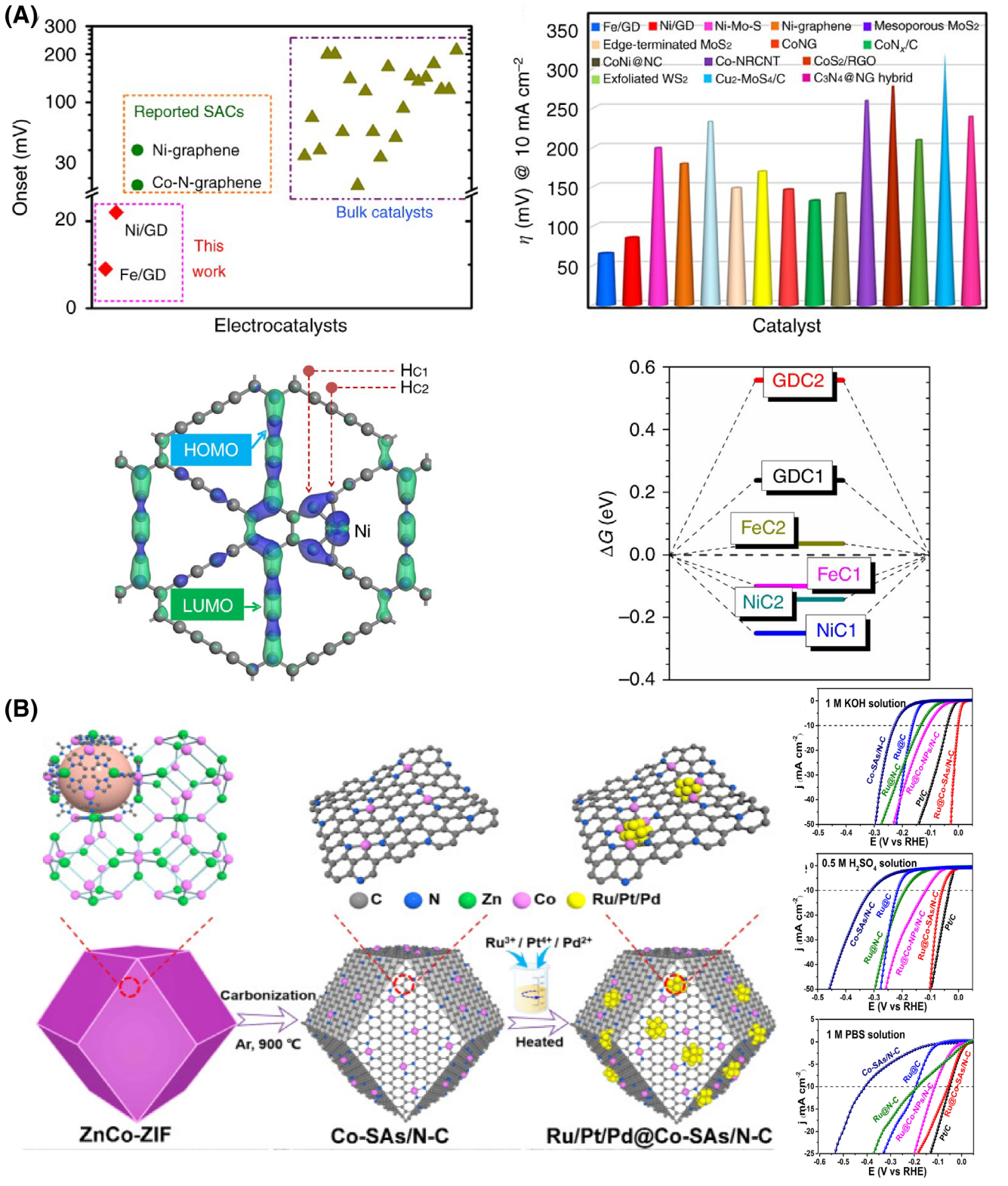

FIGURE 4 (A) The zero valence Ni and Fe single atoms anchored on graphdiyne for HER. The onset of potentials and overpotentials at the current density of 10 mA cm^{-2} of Ni/Fe-GDY catalysts are superior to other reported catalysts. Charge density analysis illustrated the strong electron transfer between metal and carbon atoms. The Ni/Fe-GDY systems have preferable adsorption strength of H. *Source:* Reprinted from Reference 17 licensed under CC-BY. (B) Schematic illustrations of the synthesis of metal clusters combined with Co-SAs/N-C single-atom catalysts and the HER activities in acidic, alkaline, and neutral conditions. *Source:* Reprinted from Reference 96 by permission from Elsevier. (C) Computational screening of G on substrates (A) MoS_2; (B) $MoSe_2$; (C) WS_2; (D) WSe_2, and correlation of φ with G_{H^*}. *Source:* Reprinted from Reference 102 by permission form the Royal Society of Chemistry

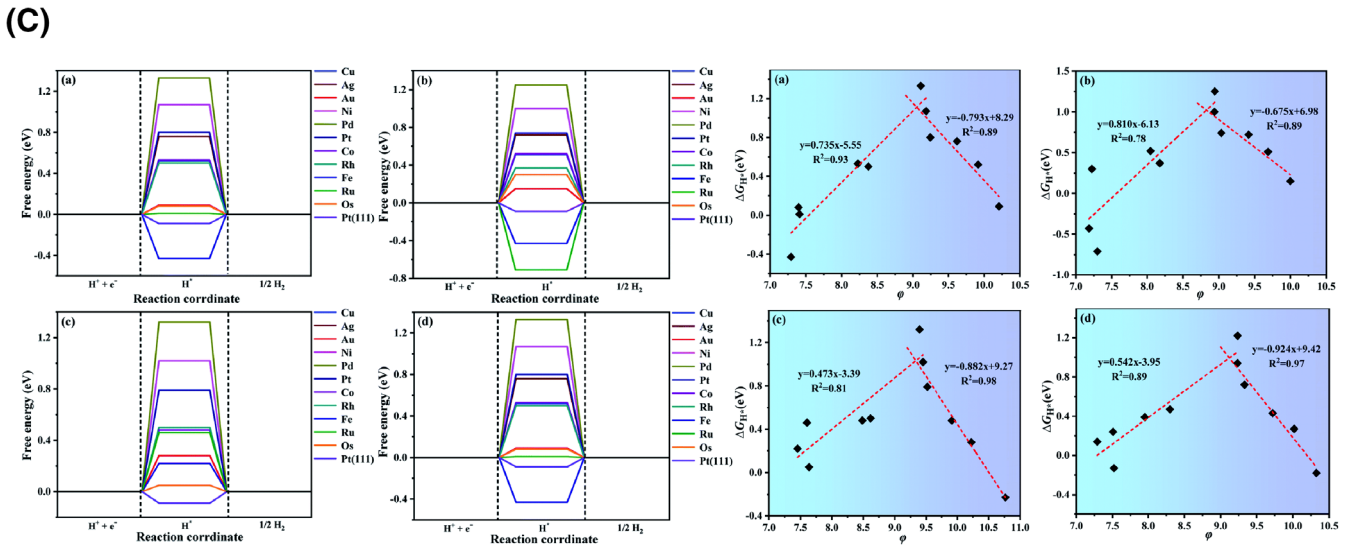

FIGURE 4 (Continued)

(Figure 4C).[102] They found that the classic d-band center theory cannot describe the bonding between the TM single atom and H accurately. Instead, the details of the partial density of states (PDOS) must be analyzed to evaluate the orbital overlap between the d-states of TM and s-states of H, which showed a high correlation with the ΔG_H. Since neither the PDOS overlap and ΔG_H are suitable for fast scanning, they proposed a new universal and efficient descriptor. As shown in Equation (6), the descriptor φ captures the number of valence electrons (θ_v), bonding distance (d), coordination number (n), and the electronegativity of the single atom site (χM) and neighboring sites (χx):

$$\varphi = \theta_V \times \left(\chi M + \sum \frac{1}{d}\chi x\right)/n \tag{6}$$

The φ descriptor demonstrates a linear relationship with ΔG_H on M-BX_2, M-AX, and ZrS_2 systems. The predictions of the descriptor are consistent with the experimental works, in particular, the Ru-MoS_2 has been confirmed to have comparable HER activity to commercial Pt/C. In summary, the recent theoretical studies on HER SACs focus on the proper descriptor of the atom site activity. Due to the unique electronic structure of SACs, the classic d-band theory meets its limit in an accurate description of the bonding ability of the metal atom. Therefore, more factors are included in the above researches, typically the electronegativity and detailed consideration of valence orbital in bonding. Meanwhile, a more efficient descriptor that requires less computational effort and conveys more intrinsic information of the SACs structure and metal element is in huge demand for the rapid screening of high HER activity transition metal SACs.

4.2 | Oxygen reduction reaction (ORR)

ORR plays a critical role in many fuel cell devices and holds a special place in the field of electrocatalysis. Oxygen is reduced to water molecules by the addition of four protons and electrons electrochemically in ORR. The multiple proton-electron transfer steps result in the complex mechanism and sluggish kinetics of ORR, which severely limits the efficiency of the fuel cell devices. Therefore, highly active electrocatalysts are demanded practical applications of ORR. Unfortunately, the currently most active commercial catalyst for ORR is the Pt/C, which suffers from the expensive cost of Pt and the unsatisfying cost-efficiency ratio.[108] Over the past decades, the development of novel ORR electrocatalysts has been a consistent hot research topic, focusing on the cheaper and more efficient Pt-alternatives, especially the non-noble metal-based catalysts.

TABLE 2 Summary of ORR single atom catalysts

Catalyst	Synthesis	Application	Overpotential (η)	Activity
Pt_1-N/BP[6]	Wet chemistry	Acidic/alkaline ORR	0.83 V	—
Cu-N-C[7]	Pyrolysis	Alkaline ORR	0.4 V	36.9 mA mg_{Cu}^{-1}
Cu SAC[8]	Pyrolysis	Alkaline ORR	0.26 V	—
SA-Fe-HPC[10]	Pyrolysis	Acidic/alkaline ORR	0.23 V	Tafel slope = 49 mV dec^{-1}
Fe-N-C[9]	MOF-derived pyrolysis	Acidic/alkaline ORR	≈0.28 V	23.27 mA cm^{-2}
Fe_{AC}@Fe_{SA}-N-C[11]	Wet chemistry	Alkaline ORR	0.40 V	61.1 mA cm^{-2}
Fe-SAs/NSC[109]	Template-assisted	Alkaline ORR	0.23 V	Tafel slope = 60 mV dec^{-1}
Co-N-C[31]	Wet chemistry	Acidic H_2O_2	0.1 V	FE = 90%
Fe-C-O[110]	Impregnation and reduction	Alkaline H_2O_2	0.122 V	FE = 95%

The recently emerging SAC is also considered as a promising candidate to achieve a high atom utilization efficiency, cheap cost as well as superior ORR activity simultaneously (Table 2). For instance, Liu et al reported a cost-effective, efficient, and durable carbon-supported Pt SAC for ORR.[6] DFT calculations suggest that the anchored Pt single atom sites are tolerant to carbon monoxide/methanol but highly active for the ORR. More importantly, the extraordinary electronic property modulation from the formation of SAC will unleash the potential of many other transition metals to become efficient ORR catalysts. Cu-based catalysts are usually excluded from the choices of ORR catalysts due to their relative inertness in the adsorption of ORR intermediates.[108,111] However, Li et al reported that the single atomic Cu anchored on nitrogen-doped two-dimensional carbon matrix (Cu–N–C) exhibited superior ORR activity compared to the Cu nanoparticles, and even surpassed the commercial Pt/C.[7] The Cu–N–C featured a high Cu content of 20.9 wt%, resulting in the abundant Cu atomic sites on the surface. The overpotential of Cu–N–C was comparable to the Pt/C, while the Tafel slope of the Cu–N–C was only 37 mV dec^{-1}, much smaller than that of Pt/C (84 mV dec^{-1}), N–C (77 mV dec^{-1}), and other state-of-the-art catalysts. DFT calculations revealed that the O_2/OOH adsorption energies of single Cu atomic sites were modulated to favorable levels and the O–O bond stretching was also improved, leading to the accelerated ORR process (Figure 5A). Cui et al also reported the synthesis of Cu SAC on CNTs through a simple pyrolysis method.[8] The ORR activity was comparable to commercial Pt/C. Fe-based catalyst has been considered as a promising candidate to replace the Pt-based ORR catalysts. However, it still suffers from poor stability and mediocre catalytic activity in acidic medium.[112] A desirable solution is to develop the Fe SAC, in which the coordinated Fe atoms will be firmly anchored on the support, typically carbon-based materials or MOF. The active site structure is typically FeN_x/C. Zhang et al developed the single Fe atom dispersed on hierarchically structured porous carbon (SA-Fe-HPC) frameworks. In acidic electrolytes, the SA-Fe-HPC catalysts exhibited comparable ORR activity to the commercial Pt/C but better long-term electrochemical stability and selectivity. In alkaline media, the SA-Fe-HPC catalysts outperformed the commercial Pt/C in both ORR activity, durability, and selectivity.[10] A MOF-based Fe-N-C SAC was synthesized by Jiao et al and demonstrated superior oxygen reduction activity and stability surpassing almost all non-noble-metal catalysts and Pt/C in both alkaline and acidic conditions.[9] The M-N-C (M = transition metal) active structure studied in Fe-based SAC catalyst has been also successfully implemented on Co and Zn, endowing satisfactory ORR activity and stability which are comparable to or even better than those of Pt-based catalysts.[65,113]

While the fabrication of SAC has been regarded as one of the promising strategies to develop highly efficient ORR catalysts, there is still room for further improvement of activity for SAC. Ao et al designed and synthesized a Fe SAC integrated with Fe nanoclusters.[11] The active sites were still the single-atom Fe sites, while the activity was remarkably enhanced under the synergistic effect from the embedded Fe nanoclusters, confirmed by experiments and theoretical calculations (Figure 5B). Zhang et al attempted to introduce the sulfur atoms to the nitrogen-doped carbon matrix (N, S-codoped carbon matrix, NSC) and investigated the catalytic performance of Fe, Co, Ni-SAC based on this support.[109] The structural analysis revealed that the S atoms form bonds with N atoms for Fe-SAs/NSC, while metal-S bonds are formed in Co-SAs/NSC and Ni-SAs/NSC. DFT calculations reveal that the FeN_4S_2 center site is more active than the CoN_3S_1 and NiN_3S_1 center sites, due to the higher charge density and lower energy barriers of the intermediates and products. The experiment results confirm that these three SACs all contribute high ORR activity while Fe-SAs/NSC is the best of all and surpasses the Pt/C.

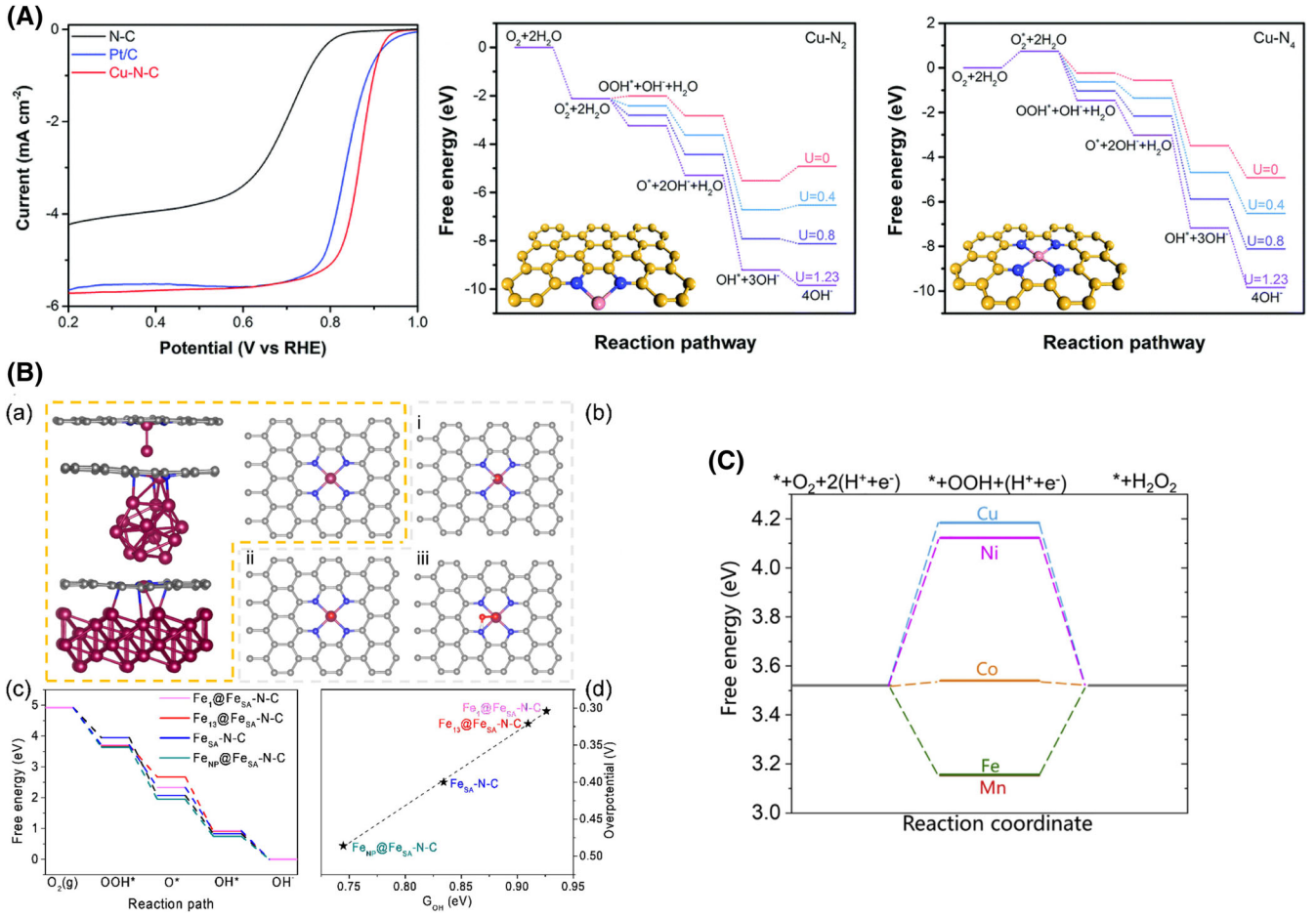

FIGURE 5 (A) Polarization curves for Cu-N-C, N-C and Pt/C in 0.1 M aq. KOH solution (oxygen saturated); reaction pathways for Cu-N_2 and Cu-N_4 sites. *Source:* Reprinted from Reference 7 by permission from the Royal Society of Chemistry. (B) Theoretical calculations of Fe_1@Fe_{SA}-N-C, Fe_{13}@Fe_{SA}-N-C, Fe_{NP}@Fe_{SA}-N-C, and Fe_{SA}-N-C. *Source:* Reprinted from Ao et al[11] by permission from the American Chemical Society. (C) Free energy diagrams of 2 e^- ORR on the SACs at $U = 0.7$ V vs RHE. *Source:* Reprinted from Reference 31 by permission from Elsevier

The ORR is not limited to its four-electron process forming water molecules from the reduction of molecular oxygen. The two-electron pathway that generates hydrogen peroxide is also under extensive research due to its broad applications and the unsatisfactory industrial production method. Electrochemical ORR offers an attractive route for direct formation of hydrogen peroxide and on-site applications. Unfortunately, the cost-effective electrochemical catalysts for two-electron ORR are still lacking. Moreover, the selectivity competition between the two-electron pathway and the four-electron pathway is also a challenge to resolve for efficient electrochemical H_2O_2 production. The O–O bond splitting ability should be suppressed to promote the two-electron pathway of ORR. SACs are therefore the promising candidates since the adsorption of oxygen molecules on a single atomic site typically takes the end-on configuration, which is not that favorable for the O–O bond splitting as the μ-peroxo coordination. Gao et al found that the Co SAC has the optimum close to zero ΔG_{OOH^*} among Mn, Fe, Co, Ni, and Cu, suggesting it has the highest catalytic activity toward the two-electron ORR pathway (Figure 5C).[31] The subsequent electrochemical tests were consistent with the theoretical prediction, showing that the Co-NC SAC even slightly outperformed the best previously reported catalysts in acidic media, the Pd-Hg alloy.[114] Jiang et al conducted a study on the two-electron ORR SACs with CNTs as the support.[110] Among the selected transition metal elements (Pd, Fe, Co, and Mn), the Fe-CNT presented the best H_2O_2 performance in terms of activity and selectivity in experiments. The DFT calculations revealed that the Fe-C-O motifs were responsible for the enhanced activity and selectivity. Comparison of the OOH* adsorption energies of different coordination motifs suggested that both Fe and O atoms in CNTs essentially contributed to the H_2O_2 catalytic performance.

Although the SAC has been demonstrated to be highly active for ORR by experiments and theoretical calculations, the detailed mechanism of the enhanced activity remains controversial. Wang et al recently presented a microkinetic model

for ORR on Fe-N-C SACs and unveiled a self-adjusting mechanism induced by its intrinsic intermediate.[115] The OH* at 0.28-1.00 V of potential on FeN_4 would form a new active moiety, $Fe(OH)N_4$. Therefore, unlike the previous assumption, the active center during the ORR of Fe-N-C is not constantly the FeN_4. The $Fe(OH)N_4$ presented the optimized intermediate bindings, owing to the electronic structure modulation induced by OH*. This unique self-adjusting mechanism will enable alternative strategies for improving the ORR activity. Besides increasing the density of single atomic sites, utilizing a proper ligand to replace OH* to optimize the electronic structure of the atomic site should be another promising choice. Therefore, the rational design of ORR SAC remains a lot of room to discover. The complex reaction mechanism of ORR also demands a more in-depth analysis, especially on the SAC with unique electronic structures and coordination environments.

4.3 | Oxygen evolution reaction (OER)

H_2 has been proposed as a future energy source under the growing concerns on environmental issues and demands for clean energy.[116] The electrochemical water-splitting is the most direct way to produce H_2, but it is hindered by the low efficiency of the counterpart reaction, OER. Being the reverse reaction of ORR, OER also suffers from the large overpotential and sluggish kinetics.[117] Therefore, catalysts with substantially high activity as well as superior stability are desired for the application of OER.[118] Currently, the benchmark OER catalysts are the noble metal oxides, IrO_2 and RuO_2, which are not satisfactory due to their scarcity and expensive cost.[119] The recently developed nanoparticle OER catalysts have already shown remarkable activity enhancement of lower overpotentials, yet their efficiency and active site utilization rate can be improved by the SAC strategy.[120] Both noble metals and non-noble metals SAC for OER have been designed, synthesized in recent years, showing substantial activity enhancements and prolonged activity compared to their oxides or nanomaterials counterparts.[120-124]

The reported SACs in electrocatalysis typically show binding with nitrogen atoms, which yields unsatisfactory OER activity.[124] Hence, modulation of the metal atom coordination is a promising strategy to improve the charge transfer and the OER activity (Table 3). Li et al reported a Ni SACs coordinated to oxygen sites on graphene-like carbon (Ni-O-G SACs) showing exceptionally excellent OER activity. The Ni-O-G SACs outperformed the state-of-the-art OER SACs in a variety of electrochemical performance parameters, including overpotential, Tafel slope, current density, and turnover frequency (TOF).[12] The Ni-O-G SACs displayed a 3D interconnected porous framework composed of ultrathin graphene-like sheets, single atomic distribution of Ni sites, Ni–O configuration, and high valence state of single Ni atoms. DFT calculations uncovered that the Ni–O bonding resulted in a high oxidation state of single Ni atoms, which leads to the low OER overpotential and reduced Gibbs-free energy (Figure 6A). Further activity improvement on Ru was explored in the Ru/CoFe-LDHs catalyst, fabricated by Li et al[13] The Ru single atoms are anchored on the surface of CoFe layered double hydroxides (CoFe-LDHs) by Ru-O-M (M = Fe or Co) bond. The Ru/CoFe-LDHs showed an overpotential as low as 198 mV at a current density of 10 mA cm^{-2}, a substantially lowered Tafel slope of 39 mV dec^{-1} and durability in alkaline solution, which outperformed both the CoFe-LDHs and commercial RuO_2. Ru single atomic sites were confirmed as the active sites for OER by in situ XAS and DFT calculations. The CoFe-LDHs worked as co-catalysts which accelerated the kinetics of the OOH* group from O* group. The strong electronic coupling between the Ru and CoFe-LDHs was observed by XPS spectra and demonstrated by differential charge density from calculation results. The electron donation from LDHs to Ru stabilized the valence states of Ru below +4, preventing the oxidation and activity loss of Ru sites and substantially enhanced the electron transfer ability. Similarly, Zhang et al explored the synergistic effect between single-atom Au and the NiFe-LDH support and found that the anchored single-atom Au successfully enhanced the Fe active sites on LDH via electron transfers and inducing charge redistribution on the Fe sites (Figure 6B).[14] Anchoring Ru atoms in the cavity of

TABLE 3 Summary of OER single atom catalysts

Catalyst	Synthesis	Application	Overpotential (η)	Activity
Ni-O-G[12]	NaCl template	Alkaline OER	224 mV at 10 mA cm^{-2}	Tafel slope = 42 mV dec^{-1}
Ru/CoFe-LDHs[13]	Wet chemistry	Alkaline OER	198 mV at 10 mA cm^{-2}	Tafel slope = 39 mV dec^{-1}
Au/NiFe-LDH[14]	Electrodeposition	Alkaline OER	237 mV at 10 mA cm^{-2}	64.8 A g^{-1}
Ru_1-Pt_3Cu[16]	Acid and electrochemical leaching	Acidic OER	220 mV at 10 mA cm^{-2}	6615 A $g_{Ru}{}^{-1}$

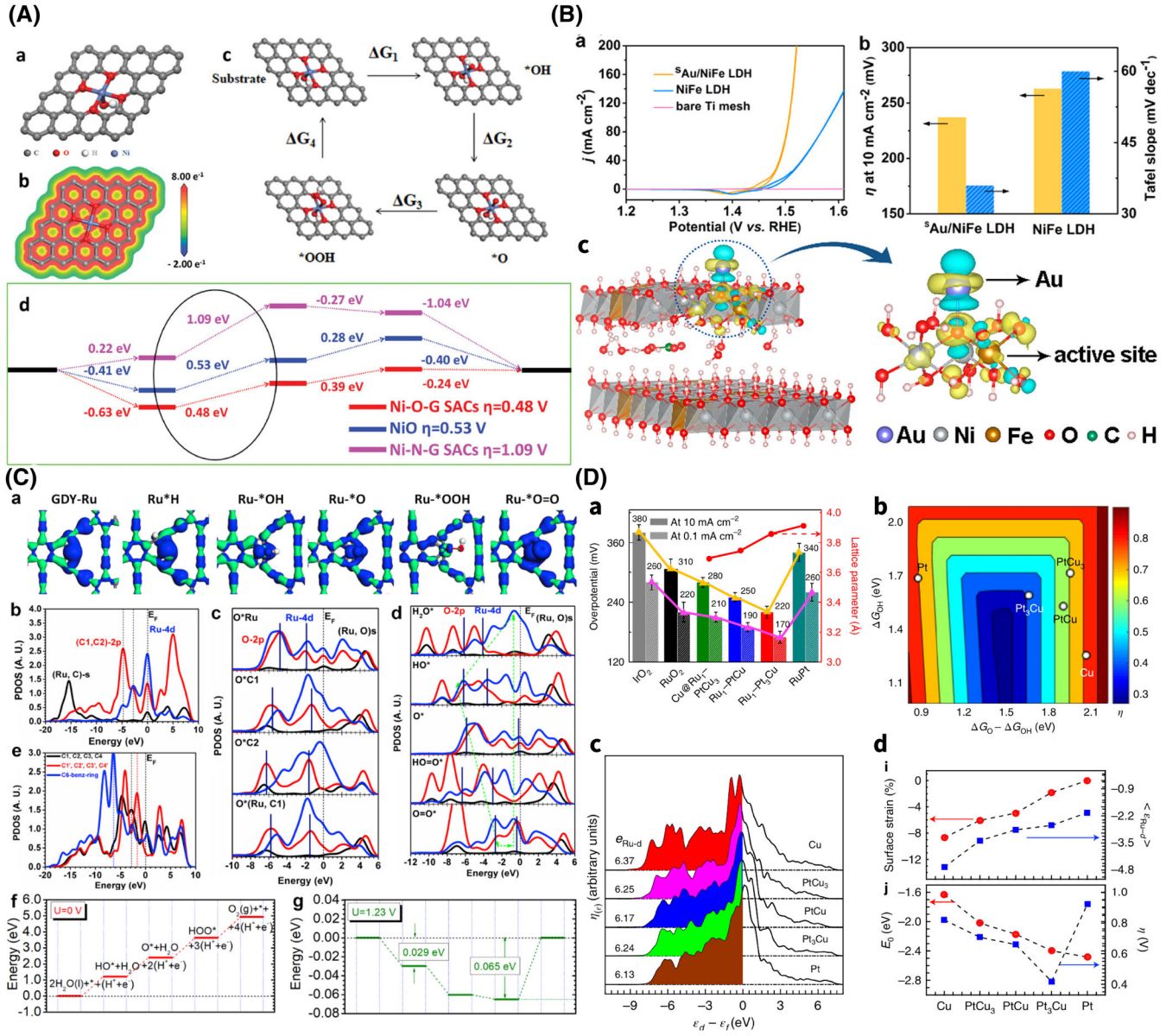

FIGURE 6 (A) DFT modeling of Ni-O-G SACs structure and free energy diagrams of OER pathways and theoretical overpotentials. *Source:* Reprinted from Reference 12 licensed under CC-BY. (B) CV curves, overpotentials, and Tafel slope comparison for ^{S}Au/NiFe LDH and pure NiFe LDH. Schematic illustration of the activation on Fe sites via Au anchoring. *Source:* Reprinted from Reference 14 by permission from the American Chemical Society. (C) Electronic structures and orbital contour plots for Ru-GDY catalysts, and the reaction pathway for OER at $U = 0$ V and $U = 1.23$ V vs RHE, respectively. *Source:* Reprinted from Reference 15 by permission from Elsevier. (D) Compressive strain effect on the OER activity of Ru single atoms embedded in PtCu alloy. *Source:* Reprinted from Reference 16 licensed under CC-BY

the novel graphdiyne material enable the bifunctional catalytic ability for water-splitting (Figure 6C).[15] The highly active electronic migration and redistribution from the site-to-site between Ru and neighboring C atom sites and adsorbates were observed, which contributed to the modulation of Ru electronic structure and consequently the enhanced HER and OER activity. The C_6 ring and the Ru neighboring C sites showed a strong electron-rich character and compensated the charge depletion from Ru-site during the electrocatalysis process. Furthermore, adsorption of protons would lead to the self-modification on the Ru-4d band, endowing the efficient electron-transfer with OER intermediates. Besides introducing other transition metal elements, the strain is also effective in modulating the electronic structure of single atomic sites, reported by a study on Ru-SAC by Yao et al (Figure 6D).[16] Although RuO_2 is reported to be one of the most active OER catalysts, it suffers from instability during the reaction. The frequent changes in the redox state of metal and formation of

Ru-O_x moieties that would peel off from defects are the major reasons for the instability. By cooperating with the Ru single atom sites on the PtCu alloys with a varied lattice constant, an OER catalyst with enhanced activity and remarkable stability is obtained. The lattice strain on the PtCu alloy was controlled by adjusting the content of Cu via sequential acid etching and electrochemical leaching. As DFT calculations analyzed, the compressive strain increased as the Cu content became higher, and the impact on the d-band was synchronously imposed on the supported Ru atom sites. The improved oxidation and dissolution resistance of the Ru_1-$PtCu_3$ catalysts was explained by the charge transfer analysis, which suggested that the gained charge on adsorbed oxygen mainly came from the Pt-Cu alloys but less from the single atomic Ru itself. This work provided a novel pathway for the electronic structure engineering of the single-atomic site, which will promote the activity as well as durability.

4.4 | Nitrogen reduction reaction (NRR)

Artificial fixation of N_2 from the atmosphere to produce NH_3 is crucial since the NH_3 is an indispensable chemical for a broad range of industries and agricultural applications.[125,126] However, the chemically inert nature of N_2 significantly hinders the conversion in mild condition, owing to the extremely high bond energy (940.95 kJ mol^{-1}) of the N≡N triple covalent bond.[127] Electrochemical reduction of N_2 to NH_3 is expected to be the solution for future ammonia production since it can operate in moderate conditions and couple with water-splitting to obtain the hydrogen and required electricity without pollution. However, due to the large energy barrier and the competitive side reaction HER, the efficiency of electrochemical NRR is still severely limited. Therefore, activation of the N≡N triple bond and suppression of HER is the key challenge to improve the yield and FE of NRR. Although extensive efforts have been made, the state-of-the-art NRR electrocatalysts still could not achieve the balance between activity and selectivity. The FE of NRR reduction is typically below 10%.[22]

SACs are considered as promising candidates for NRR electrocatalysis for its advantages of high atom utilization efficiency, unique electronic structures, and similarity of the coordination environments to the ligand fields of molecular NRR catalysts (Table 4).[128] There have been theoretical and experimental studies that demonstrated improved NRR performances by SACs in acidic or alkaline media.[21-28] Inspired by the Haber-Bosch process, Fe and Ru-based catalysts have been studied and synthesized for NRR electrocatalysis. Lü et al reported an isolated single Fe atomic sites supported on N-doped carbon frameworks (ISAS-Fe/NC) as a robust electrocatalyst for NRR in neutral media, with a FE of 18.6 ± 0.8% and a stable activity of more than 24 hours.[128] The NH_3 yield rate was up to 62.9 ± 2.7 μg $hour^{-1}$ $mg_{cat.}{}^{-1}$ at room temperature and − 0.4 V vs RHE. The DFT calculations interpreted the efficient NRR catalytic activity of the ISAS-Fe/NC as the result of substantial electron transfer from d-band of Fe to the N≡N triple bond, extending the bond length and activating it for the subsequent hydrogenation. Hence, the high density of atomically dispersed FeN_4 sites is the origin of the enhanced NRR catalytic activity. The excellent activity of Ru for NRR is demonstrated in a Ru-nitrogen-doped carbon SAC (Ru SAs/N-C) synthesized by Geng et al (Figure 7A).[27] At −0.2 V vs RHE, the Ru SAs/N-C achieves an NRR FE of 29.6% with a partial current density of −0.13 mA cm^{-2}. The yield rate of NH_3 reaches 120.9 μg_{NH3} $mg_{cat.}{}^{-1}$ $hour^{-1}$, which is 10 times higher than the highest value reported previously. According to experiments and theoretical calculations, the Ru SAs/N-C has a stronger N_2 binding than that of its nanoparticle counterpart. Besides the classic N-doped carbon support, the TM single atoms have also been anchored on other carbon-based materials to study their activities toward NRR. For instance, the g-C_3N_4, which has small holes surrounded by three nitrogen atoms and highly resembles the 3N-doped graphene, was predicted to show excellent NRR activity when coupled with Mo, V, and W[130,131] depending on the different NRR mechanisms.

TABLE 4 Summary of NRR single atom catalysts

Catalyst	Synthesis	Application	Faradaic efficiency (%)	Yield rate
ISAS-Fe/NC[128]	MOF-derived	Neutral NRR	18.6±0.8	62.9±2.7 μg h^{-1} $mg_{cat.}{}^{-1}$ at −0.4 V vs RHE
Ru SAs/N-C[27]	MOF-derived + pyrolysis	Alkaline NRR	29.6	120.9 μg_{NH3} $mg_{cat.}{}^{-1}$ h^{-1} at −0.2 V vs RHE
Mo^0/GDY[30]	Solvothermal reduction	Acidic/Neutral NRR	21	145.4 μg $mg_{cat.}{}^{-1}$ h^{-1}
Ru@ZrO_2/NC[22]	Hydrothermal	Acidic NRR	21	3.665 mg_{NH3} $mg_{Ru}{}^{-1}$ h^{-1}

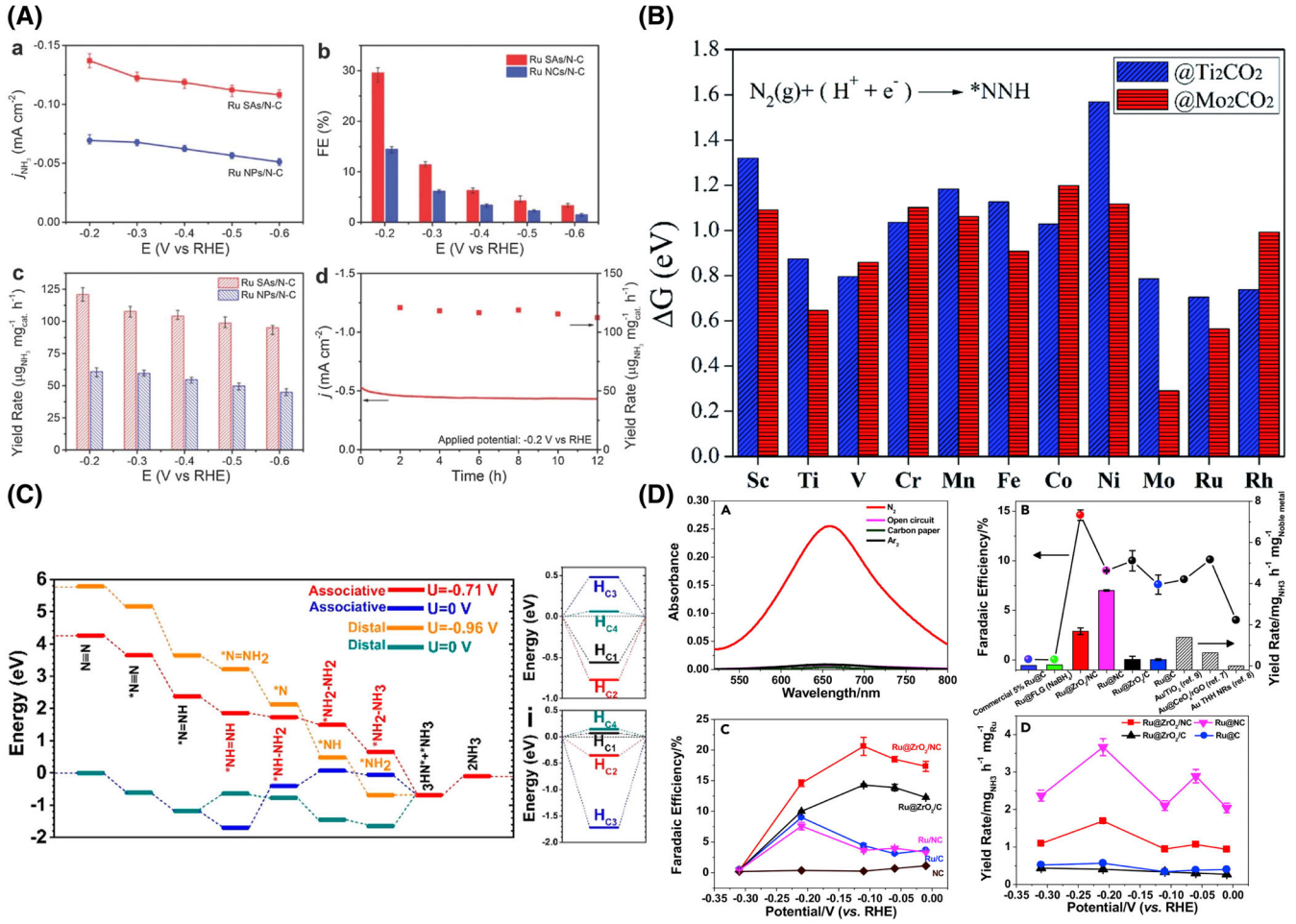

FIGURE 7 (A) NRR performance and durability of Ru SAs/N-C. *Source:* Reprinted from Reference 27 by permission from WILEY-VCH Verlag GmbH & Co. KGaA, Weinheim. (B) Reaction free energies for N_2* to NNH* on various TM@Ti_2CO_2 and TM@Mo_2CO_2, showing the Ru and Mo@Mo_2CO_2 have high selectivity to stabilize NNH*. *Source:* Reprinted from Reference 129 by permission from the Royal Society of Chemistry. (C) The reaction pathways of NRR and HER on Mo^0/GDY, demonstrating the origin of excellent NRR activity and efficient suppression of HER. *Source:* Reprinted from Reference 30 by permission from the American Chemical Society. (D) Effect of introduction of ZrO_2 to Ru SACs. *Source:* Reprinted from Reference 22 by permission from Elsevier

MXene is a novel 2D nanostructure material with the formula of $M_{n+1}X_nT_x$, in which M is a transition metal from group IIIB to VIB, X is C and/or N, T is O, OH, or F atoms, and n varies from 1 to 3. Its unique electronic properties benefit its applications in electrocatalyst, with the advantages of high surface area and better resistance to oxidation atmosphere. Therefore, Huang et al investigated the potential of single TM atoms anchored on Ti_2CO_2 and Mo_2CO_2 MXene monolayers as NRR catalysts by first principle computations (Figure 7B).[129] They reported that Ru and Mo anchored Mo_2CO_2 and Ti_2CO_2 exhibited high NRR activity, and Ru@Mo_2CO_2 had a less negative limiting potential due to the higher conductivity of Mo_2CO_2. The activity and selectivity of NRR on Mo@Mo_2CO_2 were investigated by studying the Gibbs free energy of N_2, H_2, NNH*, and H*. The results indicated that the Mo@Mo_2CO_2 could selectively stabilize NNH* in the presence of multi-dinitrogen on catalyst surfaces, endowing it the high selectivity of NRR over HER. The overpotentials of Mo@Mo_2CO_2 for NRR via distal or hybrid mechanisms were predicted to be 0.16 or 0.19 V, respectively, suggesting the rapid NRR performances. Thus, they concluded that the Mo@Mo_2CO_2 should be the potential catalyst for NRR among all the tested MXene-based catalysts. With a similar approach, Li et al conducted a theoretical screening of TM-$Mo_2TiC_2O_2$ and found that Zr-$Mo_2TiC_2O_2$ possessed the lowest barrier (0.15 eV) of the potential-determining step and high selectivity over HER.[132] Moreover, Zr-$Mo_2TiC_2O_2$ was predicted to have substantially negative formation energy, suggesting the feasibility of experimental synthesis. The recently developed new 2D carbon material, graphdiyne, features a hybrid of sp-/sp^2-hybridized carbon, was also investigated for the availability of NRR SAC. Hui et al synthesized a zerovalent Mo^0/GDY SAC, which demonstrated excellent selectivity and activity in NRR at acidic and neutral electrolytes

(Figure 7C).[30] The Mo^0/GDY exhibited an NH_3 yield rate of 145.4 μg hour^{-1} mg_{cat}^{-1} and a FE larger than 21%, which are both better than the corresponding values of previous NRR electrocatalysts. The excellent NRR activity was interpreted by DFT calculations, which unraveled that the unique C coordination with Mo in graphdiyne induced favorable electronic structure modulation of Mo-4d bands. Mo-sites and adjacent C-sites were responsible for N_2 adsorption and H adsorption, respectively. The efficient release and transfer of adsorbed H* to protonate the Nitrogen bond was the key to the activation of N_2 and suppression of HER, resulting in the high activity and selectivity of NRR. Surprisingly, it could also catalyze HER in solution without N_2 saturation via the similar principles of previously reported GDY-based HER SACs.

The recent theoretical investigations of NRR SAC candidates mainly focused on the NRR limiting potential and selectivity over HER through discussion of ΔG of N-species, and hydrogen.[133,134] Moreover, according to a theoretical screening of the adsorption energy of NRR intermediates and HER intermediates, the introduction of early-transition metals can suppress the HER.[135] Tao et al applied this principle and introduced ZrO_2 to an isolated Ru single atoms anchored on N-doped porous carbon catalyst (Ru@ZrO_2/NC), producing an efficient NRR catalyst with FE up to 21% and a low overpotential of 0.17 V.[22] The NH_3 yield rate was 3.665 mg_{NH} hour^{-1} mg_{Ru}^{-1} at −0.21 V, which is over two times higher than that of the best catalyst Au/TiO_2 reported so far (1.39 mg_{NH} hour^{-1} mg_{Au}^{-1}), with the 10 times lower loading of metal. The NRR performance comparison of NC, ZrO_2/C, ZrO_2/NC, and Ru@ZrO_2/NC demonstrated that neither NC nor ZrO_2 alone was active for NRR and the FE were also below 5% (Figure 7D). Therefore, the ZrO_2 introduced to Ru/NC substantially suppressed the HER and did not affect the NRR yield rate. DFT calculations unveiled that the Ru sites activated the N_2 while the ZrO_2 weakened the H adsorption. Therefore, this Ru SAC coupled with an early-TM HER suppressor opens a potential strategy for efficient NRR electrocatalysis.

4.5 | Carbon dioxide reduction reaction (CO_2RR)

Global warming has become one of the most serious environmental issues for human beings, and the emission of CO_2 is the major reason behind it. CO_2 is a notorious greenhouse gas, causing an increase in global average temperature, changes in climate, ocean acidification, and disruption of the carbon cycle in nature. Reducing the emission of CO_2 has become an urgent task globally. Besides limiting the production of CO_2, converting, and utilizing the CO_2 in the atmosphere is another critical approach to develop. The electrochemical CO_2 is capable of both mitigating the CO_2 emission and supplying sustainable energy to society and also tuning CO_2 into useful chemicals.[29] However, the CO_2RR process is still hampered by the lack of efficient electrocatalysts, low energy efficiency, slow reaction rate, and poor selectivity. SAC is a promising candidate for efficient CO_2RR with its multiple advantages over the conventional heterogeneous and homogeneous catalyst, for example, unique electronic structures, low-coordination number, and maximum atom utilization. In particular, many SACs present excellent CO_2 to CO selectivity and efficient suppression of the competing HER. The inherently isolated active sites of SACs are considered to be the major advantages compared to non-SACs. The activation of CO_2 on single atomic sites in the aqueous electrolyte has been confirmed experimentally and therefore the competing H_2O adsorption could be suppressed on these sites. For the nanostructured catalysts, the adsorption of CO_2 and H_2O may occur simultaneously on the continuous surface (Figure 8A).[29] Moreover, nanostructured metal-based catalysts generally possess various facets and binding sites, which often exhibit different binding strength toward CO_2, H_2O, and intermediates.

To date, most of the reported heterogeneous SACs for CO_2RR is classified into the following three types: pyrolyzed M-N-C catalysts, graphene-supported SACs, and MOFs-derived SACs (Table 5). The pyrolyzed M-N-C catalysts are facile to obtain since their precursors are low-cost and diverse and the method is suitable for large-scale synthesis and adaptable to a great variety of metals. Varela et al initially reported the Fe/Mn-containing N-doped porous carbon black heterogeneous SAC for CO_2RR, which established the pathway that using M-N-C catalysts for CO_2RR to CO.[145] Ju et al explored the M-N-C (M = Mn, Fe, Co, Ni, and Cu) SACs for the electrochemical reduction of CO_2 to CO.[139] The M-N-C materials were obtained by an impregnation process of coordinated polymer-derived N-doped porous carbons in metal chloride solution and subsequent heat treatments and acid leaching. Based on their experimental observations, the M-N_x site played the dominant role in the CO_2RR process. Co-N_x was found to be more active for HER while the Fe- and Ni-N_x SACs showed a unique reactivity and FE for reducing CO_2 into CO. The Fe-N-C displayed the maximum FE_{CO} of 65% at a low overpotential of −0.55 V vs RHE, while Ni-N-C reached the highest FE_{CO} of 85% at −0.78 V vs RHE, which outperformed the state-of-the-art Au catalyst in mass activity with a much lower cost. The subsequent DFT analysis revealed that the binding energy of intermediates could serve as descriptors for CO_2RR activity and selectivity. For instance, Co-N_x sites displayed all downhill energetics for hydrogen but severe barriers for CO formation. In contrast, the Ni-N_x required a

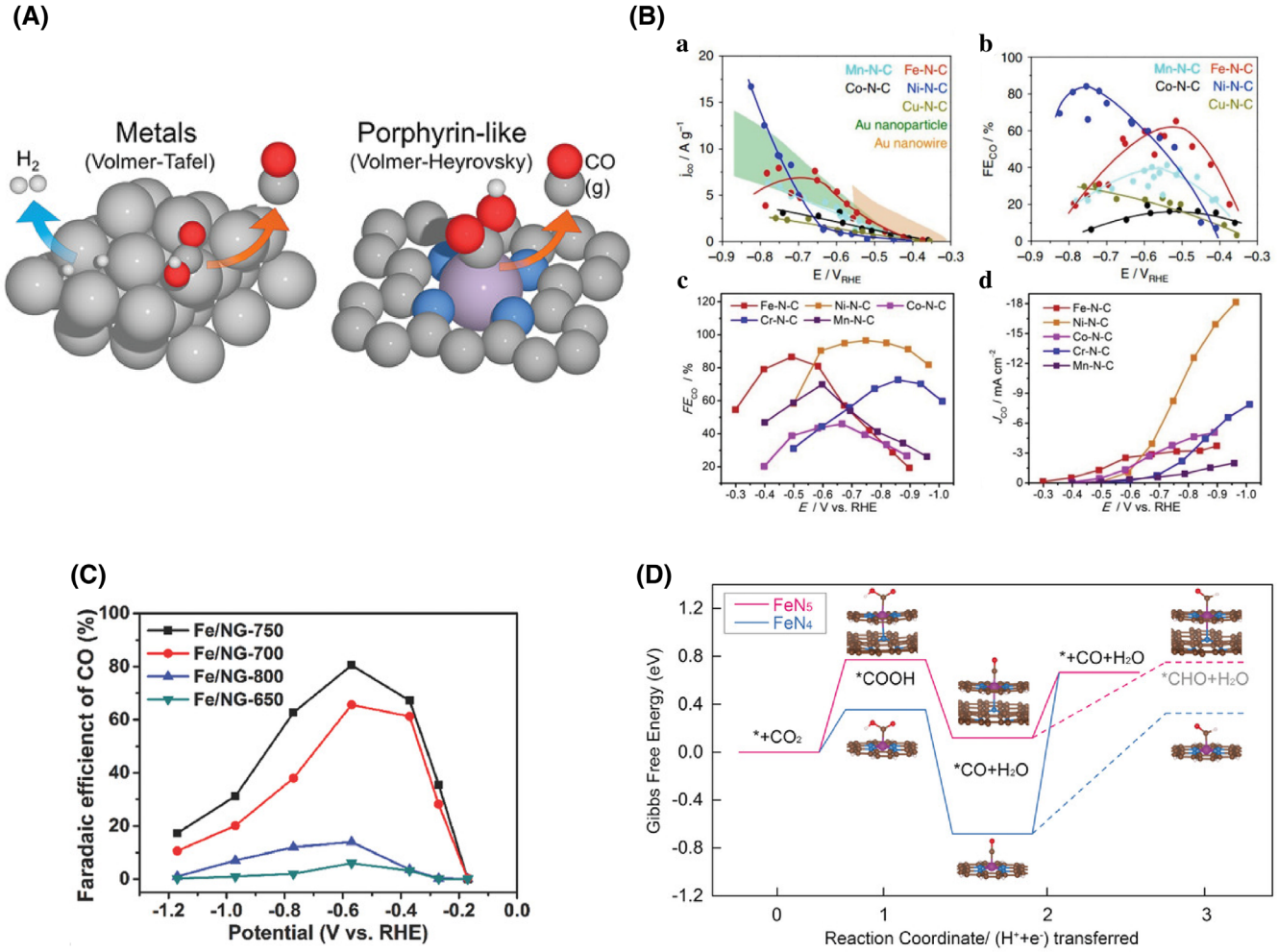

FIGURE 8 (A) Schematic illustration of CO_2 selectivity difference for SACs and nanostructured catalysts. *Source:* Reprinted from Bagger et al[136] by permission from Elsevier. (B) CO2RR performance of pyrolyzed M-N-C catalysts. *Source:* Reprinted from Li et al[29] by permission from WILEY-VCH Verlag GmbH & Co. KGaA, Weinheim. (C) FECO performance over the Fe/NG catalysts. *Source:* Reprinted from Zhang et al[137] by permission from WILEY-VCH Verlag GmbH & Co. KGaA, Weinheim. (D) Free energy profile for electroreduction of CO_2 to CO. *Source:* Reprinted from Zhang et al[138] by permission from WILEY-VCH Verlag GmbH & Co. KGaA, Weinheim

TABLE 5 Summary of CO_2RR single-atom catalysts

Catalyst	Synthesis	Application	Faradaic efficiency (%)
Fe-N-C[139]	Pyrolysis	CO_2 to CO	65 (at −0.55 V vs RHE)
Ni-N-C[140]	Pyrolysis	CO_2 to CO	96
Ni-N-Gr[141]	Heat treatment	CO_2 to CO	90 (at −0.7 to −0.9 V vs RHE)
Fe/NG-750[137]	Wet chemistry	CO_2	≈ 80 (at −0.6 V vs RHE)
FeN_5[138]	Pyrolysis	CO_2 to CO	97 (at −0.46 V vs RHE)
Ni/Fe-N-C[142]	MOF-derived	CO_2 to CO	98 (at −0.7 V vs RHE)
Sn/N-doped Graphene[143]	Quick freeze-vacuum drying-calcination	CO_2 to HCOOH	74.3 (at −0.946 V vs RHE)
CuSAs/TCNFs[144]	Wet chemistry	CO_2 to CH_3OH	44

large overpotential to initiate either the HER or CO_2RR but had a much more favorable energy pathway for CO formation. These interpretations were consistent with the experimental results. Similar trends and conclusions were supported by the work of Pan et al[140] (Figure 8B). The disadvantages of pyrolyzed M-N-C catalysts involve the less controllable process and the coordination environment is hard to precisely regulate. Graphene is a novel carbon material with 2D structure, high specific area, high electrical and thermal conductivity, and abundant surface functional groups and defects, making it a great platform to load single atom sites. The single atoms are stabilized with the bindings with N atoms in N-doped graphene and also the vacancies on graphene.[146] Su et al first reported the synthesis of a Ni and N modified graphene as an electrocatalyst for CO_2RR.[141] It was synthesized through the heat treatment of GOs and Ni-complexes at 900°C within 1 minute under an inert atmosphere. The single atomic nature of the Ni atoms coordinated with N atoms was confirmed by XPS and EXAFS results. The Ni-N sites were the active centers for the reduction of CO_2 to CO. The FE for CO formation reached 90% at −0.7 to −0.9 V vs RHE, and the TOF for CO production came up to ≈2700 hours^{-1} at −0.7 V vs RHE. The introduction of nitrogen in graphene is essential for the synthesis of graphene-supported SACs. Zhang et al demonstrated the important role of metal-nitrogen coordination in the Fe/NG-750 SAC annealed at 750°C in NH_3/Ar atmosphere.[137] The maximum FE_{CO} of ≈80% at −0.6 V vs RHE. The XAFS result and CO_2RR performance confirmed that the atomically dispersed pyridinic Fe-N_4 sites were responsible for the enhanced activity. In comparison, metallic Fe and Fe_3O_4 nanoparticles formed at a higher temperature (800°C) or with the excess amount of $FeCl_3$ exhibited poor FE_{CO} less than 10%. (Figure 8C).

The poor CO_2RR activity of Fe-free and no N-doped catalysts further emphasized that the synergistic effect between N and atomically dispersed Fe species on graphene for CO_2RR activity. The N doping could also change the morphology and coordination environment of graphene-supported SACs to eliminate the small metallic clusters.[147] The N-doped graphene could also offer an axial N ligand to form a novel Fe-N_5 site from anchoring Fe-N_4 with N ligand, reported by Zhang et al.[138] The FeN_5 catalysts had an overpotential of 0.15 V and reached the maximum FE_{CO} of 97.0% at −0.46 V vs RHE. The additional axial N ligand in FeN_5 withdrew the d electron from Fe and resulted in a higher oxidation state of the Fe atom, reducing the Fe-CO π back-donation and facilitated the CO desorption.[138] (Figure 8D) The current shortcomings of graphene-supported SACs are the low metal loading and the time-consuming graphene synthesis process. The MOFs-derived SACs utilize the outstanding CO_2 adsorption capacity of certain MOFs to improve the electrochemical activity of CO_2RR reduction.[148] The well-defined pore structures and controllable shape and size of the MOFs-derived matrix endow the accessibility of single-atom metal sites and mass transfer. The variable metal nodes and organic linkers enable the post-modification and more possible synthetic routes. The ZIF-8 MOF is a frequent choice as the SAC precursor due to the above reasons, and the SACs derived from it have been reported to exhibit excellent CO_2RR performance.[113,142,149-154]

The challenges and perspectives of SACs for CO_2RR are briefly introduced herein. First is the products of CO_2RR beyond CO. Other products like formic acid, methane, methanol, and even ethanol are more desirable with their higher energy density and corresponding SACs have been synthesized.[29] Cu-based SACs are also receiving interest for CO_2RR since they are prone to produce deep reduction products like hydrocarbons and alcohols.[144,155] Finally, future developments on the fabrication of SACs for CO_2RR are also needed to further improve the performance. The control of the coordination environment and defect engineering should contribute to tailor the optimized electronic and geometric structures of SACs.

5 | OUTLOOK AND PERSPECTIVE

The regulation of the electronic structure of SAC is also essential to the optimized performance of various electrocatalytic applications. Despite the substantial efforts in synthesizing various kinds of SACs, the studies on the electroactivity tuning of the active single atom sites are just in infancy. Zhao et al recently reviewed the electrocatalytic activity regulation strategies of M-N-C SAC for ORR.[156] According to the M-N-C structure, four aspects were discussed regarding the regulation of the center metal atoms, coordinated atoms, environmental atoms, and guest groups. For instance, the activity of SACs is predominantly determined by the center metal atom, and hence the proper choices of metal elements for specific reactions are needed to be screened and discussed. Modifications of coordinated atoms, environmental atoms, and guest groups will impose impact to the center metal atom electronic structures to a different extent, via the electron-withdrawing or donating effect or even forming new interactions with the center atoms. Zhu et al also discussed the recent advances in engineering the local coordination environments of SACs to improve catalytic performance for carbon-based and heteroatom-coordinated SACs.[157] The experimentally verified approaches for the electronic modulation of SACs include

heteroatom doping, changing the location of single-atoms on various supports, grafting foreign coordination atoms, and construction of dual metal sites. However, more in-depth insights into the structure-activity relationship are still needed, because the current simple descriptors like electronegativity are not accurate and general enough to depict the influence on the activity. In the work cooperated with Xue et al, Huang et al found that the superior HER activity of the zero-valence Ni/Fe-GDY SAC was attributed to the superexchange between the metal atoms and neighboring C atoms on GDY.[17] The charge states of the Ni/Fe atoms anchored on GDY were actually contributed from the electron compensation from the sp-orbitals of the C atoms, which activate the neighboring C sites for HER. Such more detailed and innovative theoretical analyses are welcomed for better understanding the origin of the activity of SACs and promoting the optimization of activity.

The strong metal-support interaction is the fundamental of the SACs, endowing the stability and unique electroactivity of the SAC. Without the metal-support interaction, the isolated metal atoms tend to sinter or agglomerate either by particle coalescence or by Ostwald ripening.[158,159] However, if the metal-support interaction is too strong, the atoms will be less reactive. Therefore, an appropriate combination of metals and supports and rational understandings are necessary for the stable synthesis of high activity SACs. Zhang et al investigated the metal-support interaction for Pt1-Polyoxometalate SACs, probing the effect of metal-support interaction on stability and hydrogenation activity.[160] Characterization techniques such as XANES and XPS were applied to analyze the charge interaction of Pt with support and the charge state of Pt. The SACs were also modeled for DFT calculations to study their stability and formation energy. With a combination of experimental results and DFT calculations, they found that the core main group element (P, Si) and transition metal (Mo, W) can modulate the Pt binding energy by ≈2 eV (40%). The Pt SACs are stabilized when the adsorption energy of Pt on the support is higher than the cohesive energy of Pt. The series of Pt SACs were studied for the catalysis for propanec hydrogenation to establish structure-activity relationships. Surprisingly, the measured activation energies over the tested Pt SACs were essentially the same despite the large difference in Pt binding energy. This was consistent with the DFT calculated reaction pathway and indicated that high stability and high activity are not contradictory for single-atom catalysts. The strong metal-support interaction can even be utilized to prepare the SACs, which was innovatively reported by Liu et al.[161] They synthesized Ru SACs by mixing the sub-micron RuO_2 aggregates with a $MgAl_{1.2}Fe_{0.8}O_4$ spinel. The nature of the single atom was confirmed by aberration-corrected scanning transmission electron microscopy and X-ray absorption spectroscopy. The detailed experimental analyses revealed that the dispersion of Ru atoms was an anti-Ostwald ripening process, wherein Ru atoms/RuO_2 subunits break away from static RuO_2 aggregates and diffuse across the surface and get trapped. This is driven by the strong metal-support interaction between Ru and Fe, verified by a H_2 temperature-programmed reduction (H_2-TPR) characterization. The strong metal-support interaction driven synthesis of Ru SACs was extended to the large-scale production on a kilogram scale. A 1000 g of Ru_1/Fe_2O_3 catalyst sample was obtained facilely by mixing two commercial bulk oxides and heating to 900°C. This work demonstrates the novel application of the intrinsic strong metal-support interaction in SAC and may have a profound influence on the future large-scale production of SACs.

The singly dispersed atomic active sites are the unique feature of the single-atom catalyst, which gifts the SAC with numerous excellent electrochemical properties and durability. In recent years, inspired by the SAC, similar works have been achieved in atomic modulations in nanocarbons.[162-164] However, the distinct geometry of single atomic sites sometimes is not the optimal choice, depending on the reaction mechanisms. The double atomic catalyst (DAC) is derived from the SAC, under the same genre of atomic catalysts. Instead of anchoring the metal atoms singly on the substrate, the metal atom dimers are anchored on the substrate, and the dimers are isolated as the atoms in SAC. In other words, the dimers of DAC can be view as an alternative unit of the single atom on SAC. Similar to the development of DAC, the triple atom catalysts (TACs) are synthesized. Liu et al reported a triangular Au_3 hollow active site on nanosized Au clusters can act as a promoter for the scission of the O–O bond of O_2.[165] For reactions such as alkaline OER and NRR, the monometallic single-atom catalyst is reported to be less ideal for the reactions to proceed, but the DAC and TAC could have a more favorable pathway due to the small bridge units on the surface.[28,165,166] For example, the Au_3 TAC significantly accelerates the key step of CO oxidation, the O–O bond scission in the OOCO* intermediates[165] and the TM_n-C_2N DAC activates the adsorbed N_2 molecule with the bridge sites more effectively.[28] Moreover, the monotonous active site of SACs put themselves in the limit of the linear scaling relationship between the adsorption energies of reaction intermediates. The linear scaling relationship has been considered as a huge barrier to the ultimate optimization of catalytic activity and reaction pathway.[167,168] Finally, although the atom utilization is 100%, the SACs also suffer from the relatively low metal loading, which consequently leads to the insufficient density of active sites and mass activity.

Therefore, double-, triple-, or more atomic catalysts might be the emerging research interest in the near future. They not only preserve the advantages of SAC but also boost higher metal atoms loading and more flexible active sites and geometry structures for reactions. In this way, the multi-atomic catalyst can adapt to more catalysis applications and perform an even better activity. Nonetheless, the precise control of the synthesis of DAC or multi-atomic catalyst undoubtedly remains a great challenge due to their complexity. Currently, the synthesis of DAC and even triple atomic catalyst (TAC) has been explored by some material scientists. For instance, Li et al synthesized graphene-supported Pt_2 dimers showing a striking activity for CO_2 hydrogenation.[169] Bai et al reported the Co-Fe double-atom catalyst for OER exhibiting remarkable activity and stability in alkaline conditions and outperformed other nonprecious OER catalysts in TOF.[166] Ma et al theoretically investigated the NRR on TM single-, double-, and triple-atom catalyst (TM = Mn, Fe, Co, Ni) based on graphdiyne and proposed that the Co_2@GDY would exhibit the best NRR catalytic activity with the low onset potential of −0.43 V and strong suppression of competing HER.[170] Furthermore, the SACs, DACs, and TACs are well matched to the units of the top, bridge, and hollow sites, and hence they can be used as ideal model systems to study structure-activity relationships and catalytic mechanisms at the atomic scale by theoretical calculations and *in situ* characterization technologies.[171] In summary, the essential advantages of SACs from the unique atomically dispersion active sites should be further extended to a larger but still atomic scale. The deeper complexity will bring more possibilities in the modulation of reaction barriers and pathways, resulting in novel electrocatalysts with unprecedented activity, selectivity, and durability in the future.

6 | CONCLUSION

The emergence of SACs creates a brand-new pathway to achieve the optimal balance between the cost and efficiency of electrocatalysts as it has the 100% atom utilization and excellent electroactivity. In this review, we briefly introduce the advantages of SACs and the origin of their unique properties at the beginning. The representative synthesis techniques and essential synthesis strategy are then elucidated to demonstrate the detailed steps and procedures to prevent metal atom agglomerations in synthesis. The reported experimental results of SACs as electrocatalysts for various fundamental electrochemical reactions are subsequently depicted and the rational interpretation of the enhanced activity is highlighted. Finally, the future development of SACs is briefly envisioned in the outlook section. The powerful atomic-scale catalysis will eventually lead to a great leap in the catalytic activity and also the atomic-economic green catalytic process.

ACKNOWLEDGEMENTS

The authors gratefully acknowledge the support of the Natural Science Foundation of China (Grant No.: NSFC 21771156), and the Early Career Scheme (ECS) fund (Grant No.: PolyU 253026/16P) from the Research Grants Council (RGC) in Hong Kong.

PEER REVIEW INFORMATION

Engineering Reports thanks Chunxian Guo and other anonymous reviewers for their contribution to the peer review of this work.

DATA AVAILABILITY STATEMENT

Data sharing is not applicable to this article as no new data were created or analyzed in this study.

CONFLICT OF INTEREST

The authors declare no potential conflict of interest.

AUTHOR CONTRIBUTIONS

Bolong Huang: Conceptualization; investigation; project administration; resources; supervision; writing-review and editing. **Mingzi Sun:** Formal analysis; writing-original draft. **Tong Wu:** Formal analysis; writing-original draft.

ORCID

Bolong Huang https://orcid.org/0000-0002-2526-2002

REFERENCES

1. Yang X-F, Wang A, Qiao B, Li J, Liu J, Zhang T. Single-atom catalysts: a new frontier in heterogeneous catalysis. *Acc Chem Res*. 2013;46:1740-1748.

2. Liu L, Corma A. Metal catalysts for heterogeneous catalysis: from single atoms to nanoclusters and nanoparticles. *Chem Rev*. 2018;118:4981-5079.
3. Liu Y, Tsunoyama H, Akita T, Xie S, Tsukuda T. Aerobic oxidation of cyclohexane catalyzed by size-controlled au clusters on hydroxyapatite: size effect in the Sub-2 nm regime. *ACS Catal*. 2011;1:2-6.
4. Quan Z, Wang Y, Fang J. High-index faceted noble metal nanocrystals. *Acc Chem Res*. 2013;46:191-202.
5. Wang A, Li J, Zhang T. Heterogeneous single-atom catalysis. *Nat Rev Chem*. 2018;2:65-81.
6. Liu J, Jiao M, Lu L, et al. High performance platinum single atom electrocatalyst for oxygen reduction reaction. *Nat Commun*. 2017;8:15938.
7. Li F, Han GF, Noh HJ, et al. Boosting oxygen reduction catalysis with abundant copper single atom active sites. *Energy Environ Sci*. 2018;11:2263-2269.
8. Cui L, Cui L, Li Z, et al. A copper single-atom catalyst towards efficient and durable oxygen reduction for fuel cells. *J Mater Chem A*. 2019;7:16690-16695.
9. Jiao L, Wan G, Zhang R, Zhou H, Yu SH, Jiang HL. From metal-organic frameworks to single-atom Fe implanted N-doped porous carbons: efficient oxygen reduction in both alkaline and acidic media. *Angew Chem Int Ed*. 2018;57:8525-8529.
10. Zhang Z, Sun J, Wang F, Dai L. Efficient oxygen reduction reaction (ORR) catalysts based on single iron atoms dispersed on a hierarchically structured porous carbon framework. *Angew Chem Int Ed*. 2018;57:9038-9043.
11. Ao X, Zhang W, Li Z, et al. Markedly enhanced oxygen reduction activity of single-atom Fe catalysts via integration with Fe nanoclusters. *ACS Nano*. 2019;13:11853-11862.
12. Li Y, Wu ZS, Lu P, et al. High-valence nickel single-atom catalysts coordinated to oxygen sites for extraordinarily activating oxygen evolution reaction. *Adv Sci*. 2020;7:1903089.
13. Li P, Wang M, Duan X, et al. Boosting oxygen evolution of single-atomic ruthenium through electronic coupling with cobalt-iron layered double hydroxides. *Nat Commun*. 2019;10:1711.
14. Zhang J, Liu J, Xi L, et al. Single-atom au/NiFe layered double hydroxide electrocatalyst: probing the origin of activity for oxygen evolution reaction. *J Am Chem Soc*. 2018;140:3876-3879.
15. Yu H, Hui L, Xue Y, et al. 2D graphdiyne loading ruthenium atoms for high efficiency water splitting. *Nano Energy*. 2020;72:104667.
16. Yao Y et al. Engineering the electronic structure of single atom Ru sites via compressive strain boosts acidic water oxidation electrocatalysis. *Nat Catal*. 2019;2:304-313.
17. Xue Y, Huang B, Yi Y, et al. Anchoring zero valence single atoms of nickel and iron on graphdiyne for hydrogen evolution. *Nat Commun*. 2018;9:1460.
18. Chen W, Pei J, He CT, et al. Single tungsten atoms supported on MOF-derived N-doped carbon for robust electrochemical hydrogen evolution. *Adv Mater*. 2018;30:1800396.
19. Fan L, Liu PF, Yan X, et al. Atomically isolated nickel species anchored on graphitized carbon for efficient hydrogen evolution electrocatalysis. *Nat Commun*. 2016;7:10667.
20. Sun T, Xu L, Wang D, Li Y. Metal organic frameworks derived single atom catalysts for electrocatalytic energy conversion. *Nano Res*. 2019;12:2067-2080.
21. Zhao J, Chen Z. Single Mo atom supported on defective boron nitride monolayer as an efficient Electrocatalyst for nitrogen fixation: a computational study. *J Am Chem Soc*. 2017;139:12480-12487.
22. Tao H, Choi C, Ding LX, et al. Nitrogen fixation by Ru single-atom electrocatalytic reduction. *Chem*. 2019;5:204-214.
23. Liu J-C, Ma XL, Li Y, Wang YG, Xiao H, Li J. Heterogeneous Fe_3 single-cluster catalyst for ammonia synthesis via an associative mechanism. *Nat Commun*. 2018;9:1610.
24. Li X-F, Li QK, Cheng J, et al. Conversion of dinitrogen to ammonia by FeN_3-embedded graphene. *J Am Chem Soc*. 2016;138:8706-8709.
25. Jiang Y-F, Ma XL, Lu JB, Wang JQ, Xiao H, Li J. N_2 reduction on Fe-based complexes with different supporting main-group elements: critical roles of anchor and peripheral ligands. *Small Methods*. 2019;3:1800340.
26. Han L, Liu X, Chen J, et al. Atomically dispersed molybdenum catalysts for efficient ambient nitrogen fixation. *Angew Chem Int Ed*. 2019;58:2321-2325.
27. Geng Z, Liu Y, Kong X, et al. Achieving a record-high yield rate of 120.9 for N_2 electrochemical reduction over Ru single-atom catalysts. *Adv Mater*. 2018;30:1803498.
28. Chen ZW, Yan J-M, Jiang Q. Single or double: which is the altar of atomic catalysts for nitrogen reduction reaction? *Small Methods*. 2019;3:1800291.
29. Li M et al. Heterogeneous single-atom catalysts for electrochemical CO_2 reduction reaction. *Adv Mater*. 2020;32:2001848.
30. Hui L, Xue Y, Yu H, et al. Highly efficient and selective generation of ammonia and hydrogen on a graphdiyne-based catalyst. *J Am Chem Soc*. 2019;141:10677-10683.
31. Gao J, Yang H, Huang X, et al. Enabling direct H_2O_2 production in acidic media through rational design of transition metal single atom catalyst. *Chem*. 2020;6:658-674.
32. Chen Y, Ji S, Chen C, Peng Q, Wang D, Li Y. Single-atom catalysts: synthetic strategies and electrochemical applications. *Joule*. 2018;2:1242-1264.
33. Zhong W, Tu W, Wang Z, et al. Ultralow-temperature assisted synthesis of single platinum atoms anchored on carbon nanotubes for efficiently electrocatalytic acidic hydrogen evolution. *J Energy Chem*. 2020;51:280-284.
34. Xu Y, Zhang W, Li Y, Lu P, Wu Z-S. A general bimetal-ion adsorption strategy to prepare nickel single atom catalysts anchored on graphene for efficient oxygen evolution reaction. *J Energy Chem*. 2020;43:52-57.

35. Liu W, Zhang H, Li C, Wang X, Liu J, Zhang X. Non-noble metal single-atom catalysts prepared by wet chemical method and their applications in electrochemical water splitting. *J Energy Chem*. 2020;47:333-345.
36. Li B-Q, Zhao CX, Chen S, et al. Framework-porphyrin-derived single-atom bifunctional oxygen electrocatalysts and their applications in Zn-air batteries. *Adv Mater*. 2019;31:1900592.
37. Li B-Q, Kong L, Zhao CX, et al. Expediting redox kinetics of sulfur species by atomic-scale electrocatalysts in lithium-sulfur batteries. *InfoMat*. 2019;1:533-541.
38. Jiao L, Jiang H-L. Metal-organic-framework-based single-atom catalysts for energy applications. *Chem*. 2019;5:786-804.
39. Bakandritsos A, Kadam RG, Kumar P, et al. Mixed-valence single-atom catalyst derived from functionalized graphene. *Adv Mater*. 2019;31:1900323.
40. Zhao S et al. One-pot pyrolysis method to fabricate carbon nanotube supported Ni single-atom catalysts with ultrahigh loading. *ACS Appl Energy Mater*. 2018;1:5286-5297.
41. Jones J, Xiong H, DeLaRiva AT, et al. Thermally stable single-atom platinum-on-ceria catalysts via atom trapping. *Science*. 2016;353:150-154.
42. Qu Y, Li Z, Chen W, et al. Direct transformation of bulk copper into copper single sites via emitting and trapping of atoms. *Nat Catal*. 2018;1:781-786.
43. Qu Y, Wang L, Li Z, et al. Ambient synthesis of single-atom catalysts from bulk metal via trapping of atoms by surface dangling bonds. *Adv Mater*. 2019;31:1904496.
44. Zhang Z, Feng C, Liu C, et al. Electrochemical deposition as a universal route for fabricating single-atom catalysts. *Nat Commun*. 2020;11:1215.
45. Ding S, Guo Y, Hülsey MJ, et al. Electrostatic stabilization of single-atom catalysts by ionic liquids. *Chem*. 2019;5:3207-3219.
46. Nie L et al. Activation of surface lattice oxygen in single-atom Pt/CeO_2 for low-temperature CO oxidation. *Science*. 2017;358:1419.
47. Qiao B, Wang A, Yang X, et al. Single-atom catalysis of CO oxidation using Pt_1/FeO_x. *Nat Chem*. 2011;3:634-641.
48. Yan H, Cheng H, Yi H, et al. Single-atom Pd_1/graphene catalyst achieved by atomic layer deposition: remarkable performance in selective hydrogenation of 1,3-butadiene. *J Am Chem Soc*. 2015;137:10484-10487.
49. Kong D, Wang H, Lu Z, Cui Y. $CoSe_2$ nanoparticles grown on carbon fiber paper: an efficient and stable electrocatalyst for hydrogen evolution reaction. *J Am Chem Soc*. 2014;136:4897-4900.
50. Li X, Bi W, Chen M, et al. Exclusive $Ni-N_4$ sites realize near-unity CO selectivity for electrochemical CO_2 reduction. *J Am Chem Soc*. 2017;139:14889-14892.
51. Li X, Bi W, Zhang L, et al. Single-atom Pt as co-catalyst for enhanced photocatalytic H_2 evolution. *Adv Mater*. 2016;28:2427-2431.
52. Yang S, Tak YJ, Kim J, Soon A, Lee H. Support effects in single-atom platinum catalysts for electrochemical oxygen reduction. *ACS Catal*. 2017;7:1301-1307.
53. Zhang J, Wu X, Cheong WC, et al. Cation vacancy stabilization of single- atomic-site $Pt_1/Ni(OH)_x$ catalyst for diboration of alkynes and alkenes. *Nat Commun*. 2018;9:1002.
54. Sa YJ, Seo DJ, Woo J, et al. A general approach to preferential formation of active $Fe-N_x$ sites in Fe-N/C electrocatalysts for efficient oxygen reduction reaction. *J Am Chem Soc*. 2016;138:15046-15056.
55. Chen P, Zhou T, Xing L, et al. Atomically dispersed iron-nitrogen species as electrocatalysts for bifunctional oxygen evolution and reduction reactions. *Angew Chem Int Ed*. 2017;56:610-614.
56. Han Y, Wang YG, Chen W, et al. Hollow N-doped carbon spheres with isolated cobalt single atomic sites: superior electrocatalysts for oxygen reduction. *J Am Chem Soc*. 2017;139:17269-17272.
57. Sun S, Zhang G, Gauquelin N, et al. Single-atom catalysis using Pt/graphene achieved through atomic layer deposition. *Sci Rep*. 2013;3:1775.
58. O'Neill BJ, Jackson DHK, Lee J, et al. Catalyst design with atomic layer deposition. *ACS Catal*. 2015;5:1804-1825.
59. Zhang L, Zhao ZJ, Norouzi Banis M, et al. Selective atomic layer deposition of RuO_x catalysts on shape-controlled Pd nanocrystals with significantly enhanced hydrogen evolution activity. *J Mater Chem A*. 2018;6:24397-24406.
60. Piernavieja-Hermida M, Lu Z, White A, et al. Towards ALD thin film stabilized single-atom Pd_1 catalysts. *Nanoscale*. 2016;8:15348-15356.
61. Cheng N, Stambula S, Wang D, et al. Platinum single-atom and cluster catalysis of the hydrogen evolution reaction. *Nat Commun*. 2016;7:13638.
62. Leskelä M, Ritala M. Atomic layer deposition chemistry: recent developments and future challenges. *Angew Chem Int Ed*. 2003;42:5548-5554.
63. Jeong S-J, Gu Y, Heo J, et al. Thickness scaling of atomic-layer-deposited HfO_2 films and their application to wafer-scale graphene tunnelling transistors. *Sci Rep*. 2016;6:20907.
64. Huang H, Shen K, Chen F, Li Y. Metal-organic frameworks as a good platform for the fabrication of single-atom catalysts. *ACS Catal*. 2020;10:6579-6586.
65. Yin P, Yao T, Wu Y, et al. Single cobalt atoms with precise N-coordination as superior oxygen reduction reaction catalysts. *Angew Chem Int Ed*. 2016;55:10800-10805.
66. Chen Y, Ji S, Wang Y, et al. Isolated single iron atoms anchored on N-doped porous carbon as an efficient electrocatalyst for the oxygen reduction reaction. *Angew Chem Int Ed*. 2017;56:6937-6941.
67. Marcinkowski MD, Darby MT, Liu J, et al. Pt/cu single- atom alloys as coke-resistant catalysts for efficient C-H activation. *Nat Chem*. 2018;10:325-332.

68. Chen Y, Huang Z, Ma Z, Chen J, Tang X. Fabrication, characterization, and stability of supported single-atom catalysts. *Catal Sci Technol*. 2017;7:4250-4258.
69. Li X, Yang X, Zhang J, Huang Y, Liu B. In situ/operando techniques for characterization of single-atom catalysts. *ACS Catal*. 2019;9:2521-2531.
70. Nellist PD, Pennycook SJ. Direct imaging of the atomic configuration of ultradispersed catalysts. *Science*. 1996;274:413-415.
71. Liu J et al. Advanced electron microscopy of metal-support interactions in supported metal catalysts. *ChemCatChem*. 2011;3:934-948.
72. Midgley PA, Weyland M, Thomas JM, Johnson BFG. Z-contrast tomography: a technique in three-dimensional nanostructural analysis based on Rutherford scattering. *Chem Commun*. 2001;10:907-908.
73. Wei H, Liu X, Wang A, et al. FeO_x-supported platinum single-atom and pseudo-single-atom catalysts for chemoselective hydrogenation of functionalized nitroarenes. *Nat Commun*. 2014;5:5634.
74. Yang M, Li S, Wang Y, et al. Catalytically active au-$O(OH)_x$- species stabilized by alkali ions on zeolites and mesoporous oxides. *Science*. 2014;346:1498-1501.
75. Deng D, Chen X, Yu L, et al. A single iron site confined in a graphene matrix for the catalytic oxidation of benzene at room temperature. *Sci Adv*. 2015;1:e1500462.
76. Zhang B, Asakura H, Zhang J, Zhang J, de S, Yan N. Stabilizing a $Platinum_1$ single-atom catalyst on supported phosphomolybdic acid without compromising hydrogenation activity. *Angew Chem Int Ed*. 2016;55:8319-8323.
77. Chen Y, Kasama T, Huang Z, et al. Highly dense isolated metal atom catalytic sites: dynamic formation and in situ observations. *Chem A Eur J*. 2015;21:17397-17402.
78. Jinschek JR. Advances in the environmental transmission electron microscope (ETEM) for nanoscale in situ studies of gas-solid interactions. *Chem Commun*. 2014;50:2696-2706.
79. Gai PL, Boyes ED. Advances in atomic resolution in situ environmental transmission electron microscopy and 1Å aberration corrected in situ electron microscopy. *Microsc Res Tech*. 2009;72:153-164.
80. Gai PL, Lari L, Ward MR, Boyes ED. Visualisation of single atom dynamics and their role in nanocatalysts under controlled reaction environments. *Chem Phys Lett*. 2014;592:355-359.
81. Gai PL, Boyes ED. In-situ environmental (scanning) transmission electron microscopy of catalysts at the atomic level. *J. Phys. Conf. Ser*. 2014;522:012002.
82. Liu L, Zakharov DN, Arenal R, Concepcion P, Stach EA, Corma A. Evolution and stabilization of subnanometric metal species in confined space by in situ TEM. *Nat Commun*. 2018;9:574.
83. Wei S, Li A, Liu JC, et al. Direct observation of noble metal nanoparticles transforming to thermally stable single atoms. *Nat Nanotechnol*. 2018;13:856-861.
84. Zhao J, Deng Q, Avdoshenko SM, Fu L, Eckert J, Rummeli MH. Direct in situ observations of single Fe atom catalytic processes and anomalous diffusion at graphene edges. *Proc Natl Acad Sci*. 2014;111:15641-15646.
85. Vickerman JC, Gilmore IS. *Surface Analysis: The Principal Techniques*. 2nd ed. New York, NY: John Wiley and Sons; 2009.
86. Chen Y, Huang Z, Zhou M, et al. The active sites of supported silver particle catalysts in formaldehyde oxidation. *Chem Commun*. 2016;52:9996-9999.
87. Yates JT, Worley SD, Duncan TM, Vaughan RW. Catalytic decomposition of formaldehyde on single rhodium atoms. *J Chem Phys*. 1979;70:1225-1230.
88. Matsubu JC, Yang VN, Christopher P. Isolated metal active site concentration and stability control catalytic CO_2 reduction selectivity. *J Am Chem Soc*. 2015;137:3076-3084.
89. Lang R, Li T, Matsumura D, et al. Hydroformylation of olefins by a rhodium single-atom catalyst with activity comparable to $RhCl(PPh_3)_3$. *Angew Chem Int Ed*. 2016;55:16054-16058.
90. Pei GX, Liu XY, Wang A, et al. Ag alloyed Pd single-atom catalysts for efficient selective hydrogenation of acetylene to ethylene in excess ethylene. *ACS Catal*. 2015;5:3717-3725.
91. Shan J, Liu J, Li M, Lustig S, Lee S, Flytzani-Stephanopoulos M. NiCu single atom alloys catalyze the CH bond activation in the selective non-oxidative ethanol dehydrogenation reaction. *Appl Catal Environ*. 2018;226:534-543.
92. Chu S, Majumdar A. Opportunities and challenges for a sustainable energy future. *Nature*. 2012;488:294-303.
93. Medford AJ, Vojvodic A, Hummelshøj JS, et al. From the Sabatier principle to a predictive theory of transition-metal heterogeneous catalysis. *J Catal*. 2015;328:36-42.
94. Yu H, Xue Y, Huang B, et al. Ultrathin Nanosheet of Graphdiyne-supported palladium atom catalyst for efficient hydrogen production. *iScience*. 2019;11:31-41.
95. Xue Y, Guo Y, Yi Y, et al. Self-catalyzed growth of cu@graphdiyne core-shell nanowires array for high efficient hydrogen evolution cathode. *Nano Energy*. 2016;30:858-866.
96. Yuan S, Pu Z, Zhou H, et al. A universal synthesis strategy for single atom dispersed cobalt/metal clusters heterostructure boosting hydrogen evolution catalysis at all pH values. *Nano Energy*. 2019;59:472-480.
97. Wang T et al. Carbon-rich nonprecious metal single atom electrocatalysts for CO_2 reduction and hydrogen evolution. *Small Methods*. 2019;1900210:3.
98. He Q, Tian D, Jiang H, et al. Achieving efficient alkaline hydrogen evolution reaction over a Ni_5P_4 catalyst incorporating single-atomic Ru sites. *Adv Mater*. 2020;32:1906972.
99. Wang D, Li Q, Han C, Xing Z, Yang X. Single-atom ruthenium based catalyst for enhanced hydrogen evolution. *Appl Catal Environ*. 2019;249:91-97.

100. Wang Q et al. Design of active nickel single-atom decorated MoS_2 as a pH-universal catalyst for hydrogen evolution reaction. *Nano Energy*. 2018;53:458-467.
101. Jiang K, Liu B, Luo M, et al. Single platinum atoms embedded in nanoporous cobalt selenide as electrocatalyst for accelerating hydrogen evolution reaction. *Nat Commun*. 2019;10:1743.
102. Huang H-C, Zhao Y, Wang J, et al. Rational design of an efficient descriptor for single-atom catalysts in the hydrogen evolution reaction. *J Mater Chem A*. 2020;8:9202-9208.
103. Huang B. 4f Fine-structure levels as the dominant error in the electronic structures of binary lanthanide oxides. *J Comput Chem*. 2016;37:825-835.
104. Huang B. Intrinsic deep hole trap levels in Cu_2O with self-consistent repulsive coulomb energy. *Solid State Commun*. 2016;230:49-53.
105. Huang B. Strong compensation hinders the p-type doping of ZnO: a glance over surface defect levels. *Solid State Commun*. 2016;237-238:34-37.
106. Huang B. The screened pseudo-charge repulsive potential in perturbed orbitals for band calculations by DFT+U. *Phys Chem Chem Phys*. 2017;19:8008-8025.
107. Hossain MD, Liu Z, Zhuang M, et al. Rational design of graphene-supported single atom catalysts for hydrogen evolution reaction. *Adv Energy Mater*. 2019;9:1803689.
108. Nørskov JK, Rossmeisl J, Logadottir A, et al. Origin of the overpotential for oxygen reduction at a fuel-cell cathode. *J Phys Chem B*. 2004;108:17886-17892.
109. Zhang J, Zhao Y, Chen C, et al. Tuning the coordination environment in single-atom catalysts to achieve highly efficient oxygen reduction reactions. *J Am Chem Soc*. 2019;141:20118-20126.
110. Jiang K, Back S, Akey AJ, et al. Highly selective oxygen reduction to hydrogen peroxide on transition metal single atom coordination. *Nat Commun*. 2019;10:3997.
111. Stacy J, Regmi YN, Leonard B, Fan M. The recent progress and future of oxygen reduction reaction catalysis: a review. *Renew Sustain Energy Rev*. 2017;69:401-414.
112. Wang Y-C, Lai YJ, Song L, et al. S-doping of an Fe/N/C ORR catalyst for polymer electrolyte membrane fuel cells with high power density. *Angew Chem Int Ed*. 2015;54:9907-9910.
113. Song P, Luo M, Liu X, et al. Zn single atom catalyst for highly efficient oxygen reduction reaction. *Adv Funct Mater*. 2017;27:1700802.
114. Verdaguer-Casadevall A, Deiana D, Karamad M, et al. Trends in the electrochemical synthesis of H_2O_2: enhancing activity and selectivity by electrocatalytic site engineering. *Nano Lett*. 2014;14:1603-1608.
115. Wang Y, Tang Y-J, Zhou K. Self-adjusting activity induced by intrinsic reaction intermediate in Fe-N-C single-atom catalysts. *J Am Chem Soc*. 2019;141:14115-14119.
116. Suen N-T, Hung SF, Quan Q, Zhang N, Xu YJ, Chen HM. Electrocatalysis for the oxygen evolution reaction: recent development and future perspectives. *Chem Soc Rev*. 2017;46:337-365.
117. Han L, Dong S, Wang E. Transition-metal (Co, Ni, and Fe)-based electrocatalysts for the water oxidation reaction. *Adv Mater*. 2016;28:9266-9291.
118. Suntivich J, May KJ, Gasteiger HA, Goodenough JB, Shao-Horn Y. A perovskite oxide optimized for oxygen evolution catalysis from molecular orbital principles. *Science*. 2011;334:1383-1385.
119. Seitz LC, Dickens CF, Nishio K, et al. A highly active and stable $IrO_x/SrIrO_3$ catalyst for the oxygen evolution reaction. *Science*. 2016;353:1011-1014.
120. Zhu C, Shi Q, Feng S, Du D, Lin Y. Single-atom catalysts for electrochemical water splitting. *ACS Energy Lett*. 2018;3:1713-1721.
121. Zheng Y, Jiao Y, Zhu Y, et al. Molecule-level g-C_3N_4 coordinated transition metals as a new class of electrocatalysts for oxygen electrode reactions. *J Am Chem Soc*. 2017;139:3336-3339.
122. Zhang Y et al. Atomic iridium incorporated in cobalt hydroxide for efficient oxygen evolution catalysis in neutral electrolyte. *Adv Mater*. 2018;30:170.
123. Zeng X et al. Single- atom to single-atom grafting of Pt_1 onto Fe-N_4 center: Pt_1@Fe-N-C multifunctional Electrocatalyst with significantly enhanced properties. *Adv Energy Mater*. 2018;8:1701345.
124. Fei H, Dong J, Feng Y, et al. General synthesis and definitive structural identification of MN_4C_4 single-atom catalysts with tunable electrocatalytic activities. *Nat Catal*. 2018;1:63-72.
125. Deng J, Iñiguez JA, Liu C. Electrocatalytic nitrogen reduction at Low temperature. *Joule*. 2018;2:846-856.
126. Chen JG et al. Beyond fossil fuel-driven nitrogen transformations. *Science*. 2018;360:eaar6611.
127. Andersen SZ, Čolić V, Yang S, et al. A rigorous electrochemical ammonia synthesis protocol with quantitative isotope measurements. *Nature*. 2019;570:504-508.
128. Lü F, Zhao S, Guo R, et al. Nitrogen-coordinated single Fe sites for efficient electrocatalytic N2 fixation in neutral media. *Nano Energy*. 2019;61:420-427.
129. Huang B, Li N, Ong W-J, Zhou N. Single atom-supported MXene: how single-atomic-site catalysts tune the high activity and selectivity of electrochemical nitrogen fixation. *J Mater Chem A*. 2019;7:27620-27631.
130. Zhang L, Zhao W, Zhang W, Chen J, Hu Z. Gt-C_3N_4 coordinated single atom as an efficient electrocatalyst for nitrogen reduction reaction. *Nano Res*. 2019;12:1181-1186.
131. Chen Z, Zhao J, Cabrera CR, Chen Z. Computational screening of efficient single-atom catalysts based on graphitic carbon nitride (g-C_3N_4) for nitrogen electroreduction. *Small Methods*. 2019;3:1800368.

132. Li L, Wang X, Guo H, et al. Theoretical screening of single transition metal atoms embedded in MXene defects as superior electrocatalyst of nitrogen reduction reaction. *Small Methods*. 2019;3:1900337.
133. Choi C, Back S, Kim NY, Lim J, Kim YH, Jung Y. Suppression of hydrogen evolution reaction in electrochemical N_2 reduction using single-atom catalysts: a computational guideline. *ACS Catal*. 2018;8:7517-7525.
134. Liu X, Jiao Y, Zheng Y, Jaroniec M, Qiao S-Z. Building up a picture of the electrocatalytic nitrogen reduction activity of transition metal single-atom catalysts. *J Am Chem Soc*. 2019;141:9664-9672.
135. Skúlason E, Bligaard T, Gudmundsdóttir S, et al. A theoretical evaluation of possible transition metal electro-catalysts for N_2 reduction. *Phys Chem Chem Phys*. 2012;14:1235-1245.
136. Bagger A, Ju W, Varela AS, Strasser P, Rossmeisl J. Single site porphyrine-like structures advantages over metals for selective electrochemical CO_2 reduction. *Catal Today*. 2017;288:74-78.
137. Zhang C, Yang S, Wu J, et al. Electrochemical CO_2 reduction with atomic iron-dispersed on nitrogen-doped graphene. *Adv Energy Mater*. 2018;8:1703487.
138. Zhang H, Li J, Xi S, et al. A graphene-supported single-atom FeN_5 catalytic site for efficient electrochemical CO_2 reduction. *Angew Chem Int Ed*. 2019;58:14871-14876.
139. Ju W, Bagger A, Hao GP, et al. Understanding activity and selectivity of metal-nitrogen-doped carbon catalysts for electrochemical reduction of CO_2. *Nat Commun*. 2017;8:944.
140. Pan F, Deng W, Justiniano C, Li Y. Identification of champion transition metals centers in metal and nitrogen-codoped carbon catalysts for CO_2 reduction. *Appl Catal Environ*. 2018;226:463-472.
141. Su P, Iwase K, Nakanishi S, Hashimoto K, Kamiya K. Nickel-nitrogen-modified graphene: an efficient electrocatalyst for the reduction of carbon dioxide to carbon monoxide. *Small*. 2016;12:6083-6089.
142. Ren W, Tan X, Yang W, et al. Isolated diatomic Ni-Fe metal-nitrogen sites for synergistic electroreduction of CO_2. *Angew Chem Int Ed*. 2019;58:6972-6976.
143. Zu X, Li X, Liu W, et al. Efficient and robust carbon dioxide electroreduction enabled by atomically dispersed $Sn^{\delta+}$ sites. *Adv Mater*. 2019;31:1808135.
144. Yang H, Wu Y, Li G, et al. Scalable production of efficient single-atom copper decorated carbon membranes for CO_2 electroreduction to methanol. *J Am Chem Soc*. 2019;141:12717-12723.
145. Varela AS, Ranjbar Sahraie N, Steinberg J, Ju W, Oh HS, Strasser P. Metal-doped nitrogenated carbon as an efficient catalyst for direct CO_2 electroreduction to CO and hydrocarbons. *Angew Chem Int Ed*. 2015;54:10758-10762.
146. Back S, Lim J, Kim N-Y, Kim Y-H, Jung Y. Single-atom catalysts for CO_2 electroreduction with significant activity and selectivity improvements. *Chem Sci*. 2017;8:1090-1096.
147. Jiang K, Siahrostami S, Zheng T, et al. Isolated Ni single atoms in graphene nanosheets for high-performance CO_2 reduction. *Energ Environ Sci*. 2018;11:893-903.
148. Nugent P, Belmabkhout Y, Burd SD, et al. Porous materials with optimal adsorption thermodynamics and kinetics for CO_2 separation. *Nature*. 2013;495:80-84.
149. Geng Z et al. Regulating the coordination environment of co single atoms for achieving efficient electrocatalytic activity in CO_2 reduction. *Appl Catal Environ*. 2019;240:234-240.
150. Wang X, Chen Z, Zhao X, et al. Regulation of coordination number over single co sites: triggering the efficient electroreduction of CO_2. *Angew Chem Int Ed*. 2018;57:1944-1948.
151. Yan C, Li H, Ye Y, et al. Coordinatively unsaturated nickel-nitrogen sites towards selective and high-rate CO_2 electroreduction. *Energ Environ Sci*. 2018;11:1204-1210.
152. Zhao C, Dai X, Yao T, et al. Ionic exchange of metal-organic frameworks to access single nickel sites for efficient Electroreduction of CO_2. *J Am Chem Soc*. 2017;139:8078-8081.
153. Ye Y, Cai F, Li H, et al. Surface functionalization of ZIF-8 with ammonium ferric citrate toward high exposure of Fe-N active sites for efficient oxygen and carbon dioxide electroreduction. *Nano Energy*. 2017;38:281-289.
154. Yang J, Qiu Z, Zhao C, et al. In situ thermal atomization to convert supported nickel nanoparticles into surface-bound nickel single-atom catalysts. *Angew Chem Int Ed*. 2018;57:14095-14100.
155. Wang Y, Chen Z, Han P, et al. Single-atomic cu with multiple oxygen vacancies on ceria for electrocatalytic CO_2 reduction to CH_4. *ACS Catal*. 2018;8:7113-7119.
156. Zhao C-X, Li B-Q, Liu J-N, Zhang Q. Intrinsic electrocatalytic activity regulation of M-N-C single-atom catalysts for oxygen reduction reaction. *Angew Chem Int Ed*. 2020. https://doi.org/10.1002/anie.202003917.
157. Zhu Y, Sokolowski J, Song X, He Y, Mei Y, Wu G. Engineering local coordination environments of atomically dispersed and heteroatom-coordinated single metal site electrocatalysts for clean energy-conversion. *Adv Energy Mater*. 2020;10:1902844.
158. Hansen TW, DeLaRiva AT, Challa SR, Datye AK. Sintering of catalytic nanoparticles: particle migration or Ostwald ripening? *Acc Chem Res*. 2013;46:1720-1730.
159. Ouyang R, Liu J-X, Li W-X. Atomistic theory of Ostwald ripening and disintegration of supported metal particles under reaction conditions. *J Am Chem Soc*. 2013;135:1760-1771.
160. Zhang B, Sun G, Ding S, et al. Atomically dispersed Pt_1-polyoxometalate catalysts: how does metal-support interaction affect stability and hydrogenation activity? *J Am Chem Soc*. 2019;141:8185-8197.
161. Liu K, Zhao X, Ren G, et al. Strong metal-support interaction promoted scalable production of thermally stable single-atom catalysts. *Nat Commun*. 2020;11:1263.

162. Shen Y, Peng F, Cao Y, Zuo J, Wang H, Yu H. Preparation of nitrogen and sulfur co-doped ultrathin graphitic carbon via annealing bagasse lignin as potential electrocatalyst towards oxygen reduction reaction in alkaline and acid media. *J Energy Chem*. 2019;34:33-42.
163. Huang Y et al. Atomic modulation and structure design of carbons for bifunctional electrocatalysis in metal-air batteries. *Adv Mater*. 2019;30:1803800.
164. Tang C, Wang H-F, Zhang Q. Multiscale principles to boost reactivity in gas-involving energy electrocatalysis. *Acc Chem Res*. 2018;51:881-889.
165. Liu C, Tan Y, Lin S, et al. CO self-promoting oxidation on nanosized gold clusters: triangular Au_3 active site and CO induced O-O scission. *J Am Chem Soc*. 2013;135:2583-2595.
166. Bai L, Hsu C-S, Alexander DTL, Chen HM, Hu X. A cobalt-iron double-atom catalyst for the oxygen evolution reaction. *J Am Chem Soc*. 2019;141:14190-14199.
167. Li H, Li Y, Koper MTM, Calle-Vallejo F. Bond-making and breaking between carbon, nitrogen, and oxygen in electrocatalysis. *J Am Chem Soc*. 2014;136:15694-15701.
168. Hong X, Chan K, Tsai C, Nørskov JK. How doped MoS_2 breaks transition-metal scaling relations for CO_2 electrochemical reduction. *ACS Catal*. 2016;6:4428-4437.
169. Li H, Wang L, Dai Y, et al. Synergetic interaction between neighbouring platinum monomers in CO_2 hydrogenation. *Nat Nanotechnol*. 2018;13:411-417.
170. Ma D, Zeng Z, Liu L, Huang X, Jia Y. Computational evaluation of Electrocatalytic nitrogen reduction on TM single-, double-, and triple-atom catalysts (TM = Mn, Fe, co, Ni) based on Graphdiyne monolayers. *J Phys Chem C*. 2019;123:19066-19076.
171. Chen ZW, Chen LX, Yang CC, Jiang Q. Atomic (single, double, and triple atoms) catalysis: frontiers, opportunities, and challenges. *J Mater Chem A*. 2019;7:3492-3515.

How to cite this article: Sun M, Wu T, Huang B. Designing the future atomic electrocatalyst for efficient energy systems. *Engineering Reports*. 2020;2:e12327. https://doi.org/10.1002/eng2.12327